NASA
Technical
Paper
2643

May 1987

Surface Bidirectional Reflectance Properties of Two Southwestern Arizona Deserts for Wavelengths Between 0.4 and 2.2 Micrometers

Charles H. Whitlock,
G. Carlton Purgold,
and Stuart R. LeCroy

NASA

NASA Technical Paper 2643

1987

Surface Bidirectional Reflectance Properties of Two Southwestern Arizona Deserts for Wavelengths Between 0.4 and 2.2 Micrometers

Charles H. Whitlock
and G. Carlton Purgold
Langley Research Center
Hampton, Virginia

Stuart R. LeCroy
PRC Kentron, Inc.
Hampton, Virginia

National Aeronautics
and Space Administration

Scientific and Technical Information Office

Summary

Surface bidirectional reflectance characteristics are presented for the Sonora Desert and Mohawk Valley at solar zenith angles of 13°, 31°, and 57° at wavelengths between 0.4 and 1.6 μm. Nadir reflectance values are presented for wavelengths between 0.4 and 2.2 μm for solar zenith angles of 13°, 17.5°, 27°, 31°, 45°, 57°, and 62°. Data were taken from a helicopter during May 1985 in support of an Earth Radiation Budget Experiment (ERBE), a Stratospheric Aerosol Gas Experiment (SAGE II), and an Advanced Very High Resolution Radiometer (AVHRR) satellite validation experiment.

Introduction

Validation experiments were conducted during May 1985 in the Sonora Desert and Mohawk Valley regions in association with an Earth Radiation Budget Experiment (ERBE), a Stratospheric Aerosol Gas Experiment (SAGE II), and an Advanced Very High Resolution Radiometer (AVHRR) satellite overpasses. Both surface and atmospheric optical properties were measured for eventual input to radiative transfer models. The radiative transfer models would then be used to calculate top-of-atmosphere radiance values for comparison with satellite instrument data. Such a process is not only useful for detecting degradations in postlaunch satellite performance for systems like ERBE but also could be useful for calibration of a previously uncalibrated instrument system such as the Geostationary Operational Environmental Satellite (GOES). The objective of this paper is to report the surface measurements taken in support of these validation experiments.

During these experiments, surface reflectance properties were measured from a helicopter for a variety of view directions and a number of solar zenith angles. It is the purpose of this report to present that basic data. Specifically, combinations of reflectance characteristics are presented for wavelengths between 0.4 and 2.2 μm for solar zenith angles of 13°, 17.5°, 27°, 31°, 45°, 57°, and 62°.

Measurements

Measurements were made over both the Sonora Desert and the adjacent Mohawk Valley near Yuma, Arizona (fig. 1). Helicopter flight lines were limited to U.S. territory as shown in figure 2. The desert is partially vegetated in a fairly uniform manner as shown by the photograph in figure 3. That photograph is a nadir view taken from the helicopter at an altitude of about 0.3 km (1000 ft). Figure 4 shows AVHRR band 1 reflectance of the total desert relative to the average value under the Sonora helicopter flight line for 2 different days. In spite of possibly different atmospheres for each day, spatial distribution of albedo appears quite consistent with the major part of the desert and was within 5 percent of helicopter average values. There is a bright spot (20 percent higher than average) associated with large sand dunes near the dark lava beds, however.

Instrumentation

The instruments for measuring surface reflectance were mounted on a helicopter as shown in figure 5. The system consists of two battery-powered, four-channel radiometers housed in a single package. One radiometer operates in the visible spectrum and the other covers the near-infrared region. Both radiometers are shock mounted in a single enclosure which is mounted outboard of the helicopter fuselage with a standard, external-stores rack. A remotely controlled support arm is used to allow in-flight adjustment of viewing angle. The housing also encloses a battery-powered television camera system which records the surface target on video tape and is used to position the helicopter during sensitive calibration procedures.

The visible wavelength instrument is a modified EXOTECH Model 100-A radiometer using four filters with a 0.08-μm bandwidth and wavelengths centered at 0.40, 0.55, 0.65, and 0.75 μm. Each channel has a 5° field-of-view aperture which yields a 550-m^2 ground pixel when flown at an altitude of 0.3 km. A silicon photodiode detector is mounted behind each bandpass filter which provides a constant analog signal to the onboard flight recorder.

The near-infrared instrument is a specially designed radiometer consisting of a thermoelectrically cooled lead sulphide detector, a frequency-stabilized chopper, and a four-position filter wheel. The chopped signal is fed through a phase-sensitive detector and amplifier network to provide an analog signal to the onboard flight recorder. The filters are 0.04-μm bandwidth and cover wavelengths centered at 1.05, 1.24, 1.65, and 2.2 μm. The filters are selectable in flight, and the instrument employs the same 5° field-of-view aperture system as used in the visible wavelength instrument.

The flight data acquisition system consists of two packages which are mounted on standard seat supports in the passenger section of the helicopter. Both units are battery powered and completely self-contained. The separate battery pack is strapped to D-rings in the floor so that it may be removed for fast recharging outside the helicopter.

One package consists of a Hewlett-Packard based system utilizing the Model 3421-A data acquisition

and control unit, an HP-41CV programmable calculator, and two Model 82162 thermal printers. Remote controls for both radiometers and the support arm are contained in this package.

The second package contains the video recording system consisting of a JVC Model BR-6200 cassette recorder, a Sony 5-inch monitor, and a VTG-22 timebase module for on-screen recording of time, date, and pass numbers during the flight. This unit also serves as a voice recorder during missions to record visual observations and instrument changes.

Measurement Technique

All values presented in this report were measured over a desert which was essentially dry. There had been no rain during the previous month and most small vegetation which had appeared during the winter was quite dry and withered. Following the terminology of Kriebel 1977, all data are presented in terms of reflectance factor, which is the radiance from the ground target divided by the radiance from a calibrated near-Lambertian surface (barium sulfate paint) for the same solar angle.

Unfortunately, it was not feasible to construct a Lambertian surface large enough to be directly used as a calibration target from helicopter altitude. A secondary target was used which could be seen from altitude, and that target was related to the 1- by 1-m surface painted with barium sulfate, which was subsequently calibrated by the National Bureau of Standards. For the experiments described herein, the secondary target consisted of a large sand field which had been cleared and leveled. Nadir-viewed radiance measurements of that sand and the barium sulfate plate were made with the helicopter instrument mounted on a tripod 1 m above the surface for solar zenith angles between 13° and 62°. The reflectance factor of the sand was much less than 1 and dependent on wavelength.

Flights were planned in such a manner that the desert measurements could be referenced to the barium sulfate surface through the secondary target. After takeoff, radiance measurements were first taken over the bare sand target field. Next, measurements were taken in a nadir-viewing mode along one of the flight lines shown in figure 4. Following that, the helicopter was put into a hover mode and the nose was pointed toward the Sun (0° azimuth). Measurements were made in the Sun plane as the instruments were rotated from nadir to a viewing angle of 70° from nadir in the forward direction. The helicopter was then rotated in azimuth from the Sun plane to another plane and measurements made as the instrument was lowered back to the nadir view. The process was repeated at a number of azimuths relative to the Sun plane until 180° azimuth (tail to the Sun) was reached. The helicopter then flew back to the bare sand target field where nadir measurements were repeated. Total time lapse between the beginning and the end target field measurements was approximately 1 hour.

An atmospheric transmission correction was applied to the desert data by comparing bare sand measurements made from the helicopter and measurements made from the tripod at the surface both at the beginning and end of the flight as follows:

$$L_a = (L_{sd})_h - (L_{sd})_{sf} \tag{1}$$

where L is the radiance and the subscripts a, sd, h, and sf are atmosphere, sand, helicopter, and surface, respectively; both the surface and helicopter values are for the same solar zenith angle. Then,

$$(L_d)_{sf} = (L_d)_h - L_a \tag{2}$$

where the subscript d is desert. The atmospheric correction was assumed to vary linearly from the beginning value to the end value over the 1-hour data period. For the 0.3-km observation altitude of these tests, this correction caused the reflectance factor to change between 0.002 and 0.04, depending on the day, wavelength, and solar zenith angle. The reflectance factor of the surface bare sand is

$$(R_{sd})_{sf} = \frac{(L_{sd})_{sf}}{(L_p)_{sf}} \times R_p \tag{3}$$

where R is the reflectance factor and the subscript p is paint. The reflectance factor of the surface desert is

$$(R_d)_{sf} = \frac{(L_d)_{sf}}{(L_{sd})_{sf}} \times (R_{sd})_{sf} \tag{4}$$

Again, all quantities are for a solar zenith angle the same as that for the individual desert helicopter measurement.

Accuracy

Of prime concern was measurement uncertainty due to desert nonhomogeneity and instrument system electronic effects. The magnitude of this uncertainty was assessed by taking data continuously (every 16 sec) along each flight line and performing a statistical analysis where a Gaussian distribution of noise was assumed. Each data run contained approximately 40 points for each channel of observation. Standard deviation of total uncertainty about the mean reflectance factor value is shown in figure 6

for each observation wavelength. Figure 6(a) shows the bandwidth of each channel, and figure 6(b) shows standard deviation for both the Sonora Desert and Mohawk Valley data. Mohawk Valley reflectance uncertainty is considerably higher because the surface is less homogeneous than that of the Sonora Desert. (See fig. 7.) The average Sonora reflectance uncertainty is 0.015 reflectance factor unit of which 0.004 is believed caused by the electronic data system. The data system value is based on repeat observations of the calibration-field bare sand. The average Mohawk Valley reflectance uncertainty is 0.035 reflectance unit.

This data reduction technique is not precise because the effects of atmospheric backscatter at off-nadir viewing angles are not totally compensated for. A precise correction for atmospheric effects would require a measured aerosol phase function in the mixed layer and iterative radiative transfer calculations over the 0.3-km altitude layer. To investigate magnitude of the backscatter effect, column-average calculations were made for typical optical depths and an average aerosol phase function (derived from experimental measurements of the total-column atmospheric brightness function made independent of the data presented in this report). Surface to top-of-atmosphere losses in radiance were compared for off-nadir and nadir directions. It was then assumed that most of these losses occurred in the 4-km-thick mixing layer which existed during these experiments. (Lidar data indicate low amounts of stratospheric and upper tropospheric aerosols.) The losses were multiplied by the ratio of 0.3 km to 4 km to simulate the fact that the helicopter was in the lower portion of the mixing layer. The result of this approximation is that uncompensated backscatter would cause an error in reflectance factor of less than 0.003.

Uncertainty in reflectance of the surface painted with barium sulfate, which was used as a field standard, is a problem. The plate used in the measurements was freshly painted prior to the tests. It was covered during transit to the field and when not in use. The plate was exposed to outdoor atmospheric dust and soot for a number of hours during the data period, however. It was not possible to accurately test the plate for contamination in the field. Upon return, the plate was kept covered until tested in the laboratory. The National Bureau of Standards measured hemispherical reflectance magnitudes for wavelengths between 0.4 and 2.0 μm and bidirectional reflectance distribution function for a wavelength of 0.65 μm. These data were used in conjunction with angular properties from Kimes and Kirchner 1982 to determine absolute nadir radiance reflectance for various solar angles. Values for the painted plate from this process are given in the table at the bottom of the page. Uncertainty in these values is less than 0.06 which translates into a desert reflectance factor bias error of less than 0.036. This uncertainty is caused by the fact that visible-wavelength values had to be used for off-nadir angular properties of the plate at near infrared wavelengths. These properties are known to vary with the particular painted surface (see Butner, Schutt, and Shai 1984) and should be measured at all wavelengths for the field standard used in future experiments.

Results

Sonora Nadir Reflectance

Figure 8(a) compares Sonora Desert reflectance with values from the White Sands National Monument (from Hovis 1966). Sonora values were taken in the field at a solar zenith angle of 17.5°

Solar zenith angle, deg	Nadir-viewed radiance reflectance of painted plate at wavelength, μm, of—							
	0.40	0.55	0.65	0.75	1.05	1.24	1.65	2.20
13.0	0.971	0.970	0.966	0.959	0.944	0.939	0.915	0.861
17.5	0.971	0.970	0.966	0.959	0.944	0.939	0.915	0.861
27.0	0.961	0.960	0.956	0.949	0.934	0.930	0.905	0.852
31.0	0.951	0.951	0.946	0.940	0.925	0.920	0.896	0.843
45.0	0.916	0.915	0.911	0.905	0.890	0.886	0.863	0.812
57.0	0.869	0.868	0.864	0.859	0.845	0.841	0.819	0.770
62.0	0.825	0.825	0.821	0.816	0.802	0.798	0.778	0.732

when the sand was dry (0.16 percent soil moisture by weight). The White Sands data are from laboratory measurements of natural sand which had been shipped from the field and then a portion of the material dried in an oven. It is evident that soil moisture has a significant effect on nadir reflectance of the White Sands material.

Laboratory measurements of reflectance were performed on sand from the Sonora Desert in order to assess the effect of soil moisture on that material. Figure 8(b) shows results of those tests. The loss in reflectance is a nonlinear function of soil moisture and varies with wavelength. Like the White Sands material, soil moisture has a significant effect on Sonora reflectance. A value of soil moisture of 16 percent (by weight) reduces reflectance by approximately 50 percent. As noted previously, all data in this report were taken over dry sand.

Figure 9(a) shows the spectral variation of the nadir reflectance factor for the natural desert (sand with vegetation) for several solar zenith angles. Figure 9(b) shows variation with solar zenith angle for several wavelengths. There is significant loss in reflectance at large solar zenith angles for all wavelengths above 0.55 μm.

Figure 10 shows bare sand (secondary target) nadir reflectance factor as a function of both wavelength and solar zenith angle. Again, there is a reduction in nadir reflectance as solar zenith angle increases; however, the effect is not as large as that for the vegetated desert.

Figure 11 shows the effect of vegetation on bare sand reflectance calculated from the present data. Figure 11(a) is the ratio of vegetation to sand reflectances and shows a loss in signal below 1.2 μm in wavelength. Such an effect appears typical of both dead and live vegetation based on generalized data published by Billings and Morris 1951, Gausman et al. 1976, and Siegal and Goetz 1977. The spectral characteristic of the vegetated-to-sand reflectance ratio suggests that vegetation consisted of a mixture of both live and dead leaves with little dry sage. That conclusion is based on the fact that the ratio is less than 1 at wavelengths between 0.75 and 1.2 μm (indicating some dead vegetation) and above 1 at wavelengths between 1.2 and 1.8 μm (suggesting some live vegetation). The fact that the ratio is close to 1 at wavelengths above 1.8 μm indicates little dry sage. This type of condition is consistent with ground-level photographic evidence (fig. 12) as well as climatology factors. The desert had received excessive rain during the winter of 1984–1985 and much small vegetation had appeared. By May 1985, most of the new vegetation was dead or dying on top of the ground as a mixture with the large creosote bushes that appear stable. The important point is that the Sonora Desert vegetation is variable from year to year and month to month depending on prior rainfall. Nadir-viewed reflectance measurements are required whenever an accurate knowledge of reflectance factor is needed.

Sonora Bidirectional Reflectance

Bidirectional reflectance factor data are given in figure 13 for a solar zenith angle of 13°. For each wavelength, values are given in the upper plots for the Sun plane looking away from and toward the Sun (backward and forward reflection, respectively). In the lower plots, values are given as a function of azimuth from the Sun plane for various off-nadir angles. Where off-nadir curves are too close to be distinguished, precise values may be obtained from table 1. Zero azimuth is looking into the Sun, that is, observing forward reflected radiation. Figures 14 and 15 present the same type of results for solar zenith angles of 31° and 57°, respectively. Tables 2 and 3 give tabulated values for these conditions.

Hemispherical albedo values were obtained by integration of reflectance factor values relative to the horizontal surface. These values are also given in the tables for each wavelength. The ratio of reflectance factor to hemispherical albedo was calculated for various view and azimuth angles. Typical values are shown in figure 16 for one wavelength (0.55 μm) and two solar zenith angles (13° and 57°). Brief review indicates that solar angle has an important effect on bidirectional reflectance characteristics, and its effect is dramatic at large solar zenith angles. In the Sun plane, there is a bright spot in the direction of the Sun; this suggests a small component of direct backward reflection. At low solar zenith angles, there is little change with azimuth; however, azimuth variation increases at larger Sun angles.

Mohawk Nadir Reflectance

As noted previously, one mission was flown over the Mohawk Valley for purposes of providing information for comparison with U-2 airplane overpass data. That test made measurements over a limited range of wavelengths between 0.4 and 1.04 μm. These results are shown in figure 17. Considerable uncertainty exists with this set of data because of surface nonhomogeneity, as was previously discussed. Surprisingly, averaged data were reasonably close to Sonora values. It is also interesting to note that the data differences agree with satellite measurements. At 0.65 μm, the lower plot shows the Mohawk reflectance factor to be about 9 percent lower than helicopter-line Sonora values. Both AVHRR scenes

in figure 4 show a similar loss in signal when average values along the two helicopter flight lines are compared.

Mohawk Bidirectional Reflectance

Figure 18 presents bidirectional reflectance data in the same form as used with Sonora values. Table 4 gives tabulated reflectance factor and albedo values for the Mohawk Valley. Azimuth variations are similar to those observed for the Sonora data. The direct backward reflection component in the Sun plane is significantly larger, however. The reason for this increase is unknown.

Concluding Remarks

Surface nadir and bidirectional reflectance factors are presented for wavelengths between 0.4 and 2.2 μm and solar zenith angles between 13° and 62°. In general, reflectance factor varied between 0.12 at 0.4 μm and 0.56 at 2.2 μm. Uncertainty averaged 0.015 for the Sonora Desert and 0.035 for the Mohawk Valley as a result of surface nonhomogeneity and instrument system noise. Uncompensated atmospheric backscatter causes an uncertainty of less than 0.003 for large off-nadir viewing angles. Imperfections in the field standard for barium sulfate painted plate cause a bias uncertainty of less than 0.036.

NASA Langley Research Center
Hampton, VA 23665-5225
March 26, 1987

References

Billings, W. D.; and Morris, Robert J. 1951: Reflection of Visible and Infrared Radiation From Leaves of Different Ecological Groups. *American J. Bot.*, vol. 38, May, pp. 327–331.

Butner, Cyrus L.; Schutt, John B.; and Shai, Michael C. 1984: Comparison of the Reflectance Characteristics of Polytetrafluoroethylene and Barium Sulfate Paints. *Appl. Opt.*, vol. 23, no. 8, Apr. 15, pp. 1139–1140.

Gausman, H. W.; Everitt, J. H.; Gerbermann, A. H.; and Escobar, D. E. 1976: Leaf Spectral Characteristics of Nine Woody Plant Species From Texas Rangelands. *Remote Sensing of Earth Resources*, Volume V, F. Shahrokhi, ed., Univ. of Tennessee Space Inst., pp. 333–347.

Hovis, W. A. 1966: Infrared Spectral Reflectance of Some Common Minerals. *Appl. Opt.*, vol. 5, no. 2, Feb., pp. 245–248.

Kimes, D. S.; and Kirchner, J. A. 1982: Irradiance Measurement Errors Due to the Assumption of a Lambertian Reference Panel. *Remote Sens. Environ.*, vol. 12, no. 2, May, pp. 141–149.

Kriebel, Karl Theodor 1977: *Reflection Properties of Vegetated Surfaces: Tables of Measured Spectral Biconical Reflectance Factors.* Wiss.liche Mitt. Nr. 29, Meteorologisches Institut, Universität München, Sept.

Siegal, Barry S.; and Goetz, Alexander F. H. 1977: Effect of Vegetation on Rock and Soil Type Discrimination. *Photogramm. Eng. & Remote Sens.* vol. 43, no. 2, Feb., pp. 191–196.

Table 1. Sonora Desert Reflectance Factor for Solar Zenith Angle of 13°

Azimuth, deg	Off-nadir angle, deg	Reflectance factor at wavelength, μm, of—				
		0.4	0.55	0.65	0.75	1.65
0	0	0.123	0.269	0.354	0.424	0.539
14	0	0.123	0.269	0.354	0.424	0.539
29	0	0.123	0.269	0.354	0.424	0.539
59	0	0.123	0.269	0.354	0.424	0.539
79	0	0.123	0.269	0.354	0.424	0.539
104	0	0.123	0.269	0.354	0.424	0.539
149	0	0.123	0.269	0.354	0.424	0.539
166	0	0.123	0.269	0.354	0.424	0.539
180	0	0.123	0.269	0.354	0.424	0.539
0	15	0.108	0.243	0.324	0.393	0.496
14	15	0.108	0.243	0.324	0.393	0.496
29	15	0.111	0.247	0.329	0.396	0.503
59	15	0.111	0.252	0.332	0.401	0.516
79	15	0.118	0.256	0.334	0.403	0.514
104	15	0.126	0.260	0.336	0.405	0.512
149	15	0.123	0.268	0.347	0.418	0.532
166	15	0.126	0.277	0.363	0.433	0.554
180	15	0.126	0.277	0.363	0.433	0.554
0	30	0.107	0.241	0.320	0.388	0.492
14	30	0.107	0.241	0.320	0.388	0.492
29	30	0.115	0.246	0.324	0.387	0.488
59	30	0.111	0.246	0.323	0.390	0.497
79	30	0.115	0.253	0.332	0.400	0.507
104	30	0.119	0.261	0.342	0.411	0.516
149	30	0.123	0.266	0.350	0.420	0.530
166	30	0.118	0.263	0.347	0.416	0.532
180	30	0.118	0.263	0.347	0.416	0.532
0	45	0.115	0.243	0.317	0.378	0.481
14	45	0.115	0.243	0.317	0.378	0.481
29	45	0.122	0.251	0.326	0.386	0.481
59	45	0.120	0.248	0.321	0.384	0.489
79	45	0.120	0.252	0.328	0.392	0.498
104	45	0.119	0.257	0.335	0.400	0.507
149	45	0.123	0.262	0.344	0.410	0.517
166	45	0.120	0.260	0.340	0.404	0.517
180	45	0.120	0.260	0.340	0.404	0.517
0	60	0.124	0.241	0.306	0.357	0.457
14	60	0.124	0.241	0.306	0.357	0.457
29	60	0.121	0.243	0.313	0.366	0.468
59	60	0.119	0.241	0.308	0.364	0.472
79	60	0.122	0.242	0.310	0.366	0.463
104	60	0.124	0.243	0.312	0.368	0.454
149	60	0.124	0.256	0.328	0.386	0.490
166	60	0.117	0.246	0.318	0.374	0.486
180	60	0.117	0.246	0.318	0.374	0.486
0	70	0.128	0.227	0.284	0.330	0.422
14	70	0.128	0.227	0.284	0.330	0.422
29	70	0.127	0.226	0.282	0.326	0.426
59	70	0.126	0.230	0.290	0.336	0.438
79	70	0.127	0.234	0.295	0.343	0.442
104	70	0.128	0.237	0.300	0.350	0.445
149	70	0.133	0.251	0.318	0.369	0.478
166	70	0.125	0.238	0.301	0.350	0.452
180	70	0.125	0.238	0.301	0.350	0.452
Albedo		0.121	0.250	0.324	0.384	0.489

Table 2. Sonora Desert Reflectance Factor for Solar Zenith Angle of 31°

Azimuth, deg	Off-nadir angle, deg	Reflectance factor at wavelength, μm, of—				
		0.4	0.55	0.65	0.75	1.65
0	0	0.102	0.238	0.325	0.423	0.478
14	0	0.102	0.238	0.325	0.423	0.478
29	0	0.102	0.238	0.325	0.423	0.478
59	0	0.102	0.238	0.325	0.423	0.478
79	0	0.102	0.238	0.325	0.423	0.478
104	0	0.102	0.238	0.325	0.423	0.478
166	0	0.102	0.238	0.325	0.423	0.478
180	0	0.102	0.238	0.325	0.423	0.478
0	15	0.096	0.230	0.315	0.411	0.457
14	15	0.096	0.230	0.315	0.411	0.457
29	15	0.098	0.231	0.316	0.411	0.454
59	15	0.097	0.233	0.320	0.416	0.473
79	15	0.097	0.231	0.316	0.412	0.475
104	15	0.097	0.229	0.313	0.408	0.477
166	15	0.128	0.273	0.362	0.469	0.524
180	15	0.128	0.273	0.362	0.469	0.524
0	30	0.098	0.228	0.310	0.403	0.451
14	30	0.098	0.228	0.310	0.403	0.451
29	30	0.102	0.236	0.321	0.418	0.453
59	30	0.099	0.231	0.312	0.405	0.451
79	30	0.100	0.232	0.315	0.408	0.460
104	30	0.102	0.234	0.318	0.411	0.470
166	30	0.123	0.273	0.366	0.475	0.521
180	30	0.123	0.273	0.366	0.475	0.521
0	60	0.113	0.234	0.306	0.389	0.435
14	60	0.113	0.234	0.306	0.389	0.435
29	60	0.114	0.242	0.317	0.401	0.452
59	60	0.116	0.240	0.314	0.396	0.443
79	60	0.117	0.242	0.317	0.401	0.452
104	60	0.119	0.244	0.319	0.405	0.460
166	60	0.134	0.265	0.346	0.440	0.496
180	60	0.134	0.265	0.346	0.440	0.496
Albedo		0.114	0.245	0.325	0.417	0.468

Table 3. Sonora Desert Reflectance Factor for Solar Zenith Angle of 57°

Azimuth, deg	Off-nadir angle, deg	Reflectance factor at wavelength, μm, of—				
		0.4	0.55	0.65	0.75	1.65
0	0	0.109	0.240	0.322	0.369	0.459
14	0	0.109	0.240	0.322	0.369	0.459
29	0	0.109	0.240	0.322	0.369	0.459
59	0	0.109	0.240	0.322	0.369	0.459
79	0	0.109	0.240	0.322	0.369	0.459
104	0	0.109	0.240	0.322	0.369	0.459
149	0	0.109	0.240	0.322	0.369	0.459
166	0	0.109	0.240	0.322	0.369	0.459
180	0	0.109	0.240	0.322	0.369	0.459
0	15	0.113	0.237	0.317	0.363	0.448
14	15	0.113	0.237	0.317	0.363	0.448
29	15	0.111	0.235	0.314	0.360	0.453
59	15	0.107	0.230	0.308	0.353	0.447
79	15	0.110	0.238	0.320	0.369	0.464
104	15	0.115	0.247	0.333	0.383	0.479
149	15	0.116	0.258	0.344	0.397	0.483
166	15	0.120	0.258	0.347	0.399	0.485
180	15	0.120	0.258	0.347	0.399	0.485
0	30	0.120	0.244	0.323	0.369	0.456
14	30	0.120	0.244	0.323	0.369	0.456
29	30	0.116	0.235	0.312	0.356	0.446
59	30	0.112	0.234	0.315	0.358	0.447
79	30	0.116	0.247	0.328	0.369	0.468
104	30	0.121	0.259	0.349	0.399	0.492
149	30	0.129	0.272	0.362	0.416	0.514
166	30	0.131	0.274	0.366	0.421	0.509
180	30	0.131	0.274	0.366	0.421	0.509
0	45	0.149	0.282	0.346	0.397	0.479
14	45	0.147	0.269	0.346	0.397	0.479
29	45	0.135	0.255	0.332	0.380	0.458
59	45	0.126	0.248	0.326	0.368	0.458
79	45	0.126	0.247	0.337	0.378	0.459
104	45	0.135	0.269	0.364	0.411	0.506
149	45	0.152	0.302	0.399	0.447	0.555
166	45	0.154	0.313	0.409	0.466	0.567
180	45	0.154	0.313	0.409	0.466	0.567
0	60	0.192	0.380	0.467	0.468	0.549
14	60	0.183	0.364	0.455	0.456	0.541
29	60	0.166	0.289	0.359	0.392	0.505
59	60	0.147	0.256	0.334	0.373	0.457
79	60	0.139	0.252	0.337	0.374	0.459
104	60	0.148	0.274	0.355	0.398	0.495
149	60	0.178	0.333	0.423	0.473	0.588
166	60	0.183	0.352	0.448	0.500	0.623
180	60	0.183	0.352	0.448	0.500	0.632
0	70	*0.395	0.487	0.562	*0.816	0.590
14	70	*0.388	0.480	0.562	*0.801	0.581
29	70	*0.358	0.452	0.549	*0.694	0.540
59	70	0.187	0.262	0.315	0.351	0.428
79	70	0.148	0.247	0.311	0.348	0.438
104	70	0.163	0.277	0.349	0.388	0.486
149	70	0.210	0.351	0.434	0.479	0.614
166	70	0.216	0.371	0.459	0.507	0.652
180	70	0.216	0.371	0.459	0.507	0.663
Albedo		0.155	0.283	0.366	0.419	0.501

*Questionable data.

Table 4. Mohawk Valley Reflectance Factor for Solar Zenith Angle of 21°

Azimuth, deg	Off-nadir angle, deg	Reflectance factor at wavelength, μm, of—				
		0.4	0.55	0.65	0.75	1.04
0	0	0.110	0.216	0.291	0.368	0.460
15	0	0.110	0.216	0.291	0.368	0.460
45	0	0.110	0.216	0.291	0.368	0.460
90	0	0.110	0.216	0.291	0.368	0.460
135	0	0.110	0.216	0.291	0.368	0.460
180	0	0.110	0.216	0.291	0.368	0.460
0	15	0.123	0.224	0.294	0.362	0.440
15	15	0.106	0.204	0.269	0.339	0.427
45	15	0.092	0.199	0.269	0.355	0.440
90	15	0.100	0.200	0.269	0.346	0.454
135	15	0.115	0.235	0.310	0.389	0.484
180	15	0.166	0.304	0.382	0.454	0.541
0	30	0.119	0.216	0.286	0.357	0.439
15	30	0.091	0.176	0.253	0.327	0.408
45	30	0.085	0.176	0.258	0.336	0.425
90	30	0.097	0.189	0.260	0.336	0.432
135	30	0.123	0.239	0.315	0.394	0.489
180	30	0.135	0.251	0.331	0.410	0.512
0	45	0.097	0.179	0.243	0.313	0.399
15	45	0.088	0.171	0.242	0.316	0.408
45	45	0.098	0.195	0.274	0.349	0.430
90	45	0.109	0.202	0.269	0.339	0.433
135	45	0.135	0.249	0.317	0.392	0.482
180	45	0.116	0.216	0.287	0.365	0.476
0	60	0.101	0.182	0.251	0.321	0.405
15	60	0.097	0.181	0.251	0.326	0.412
45	60	0.109	0.193	0.257	0.324	0.421
90	60	0.103	0.190	0.257	0.327	0.425
135	60	0.119	0.216	0.280	0.352	0.465
180	60	0.106	0.216	0.292	0.375	0.490
0	70	0.110	0.181	0.242	0.310	0.398
15	70	0.101	0.167	0.225	0.299	0.391
45	70	0.098	0.160	0.218	0.292	0.389
90	70	0.112	0.184	0.244	0.311	0.411
135	70	0.104	0.191	0.256	0.329	0.439
180	70	0.113	0.200	0.264	0.338	0.453
Albedo		0.108	0.205	0.275	0.349	0.446

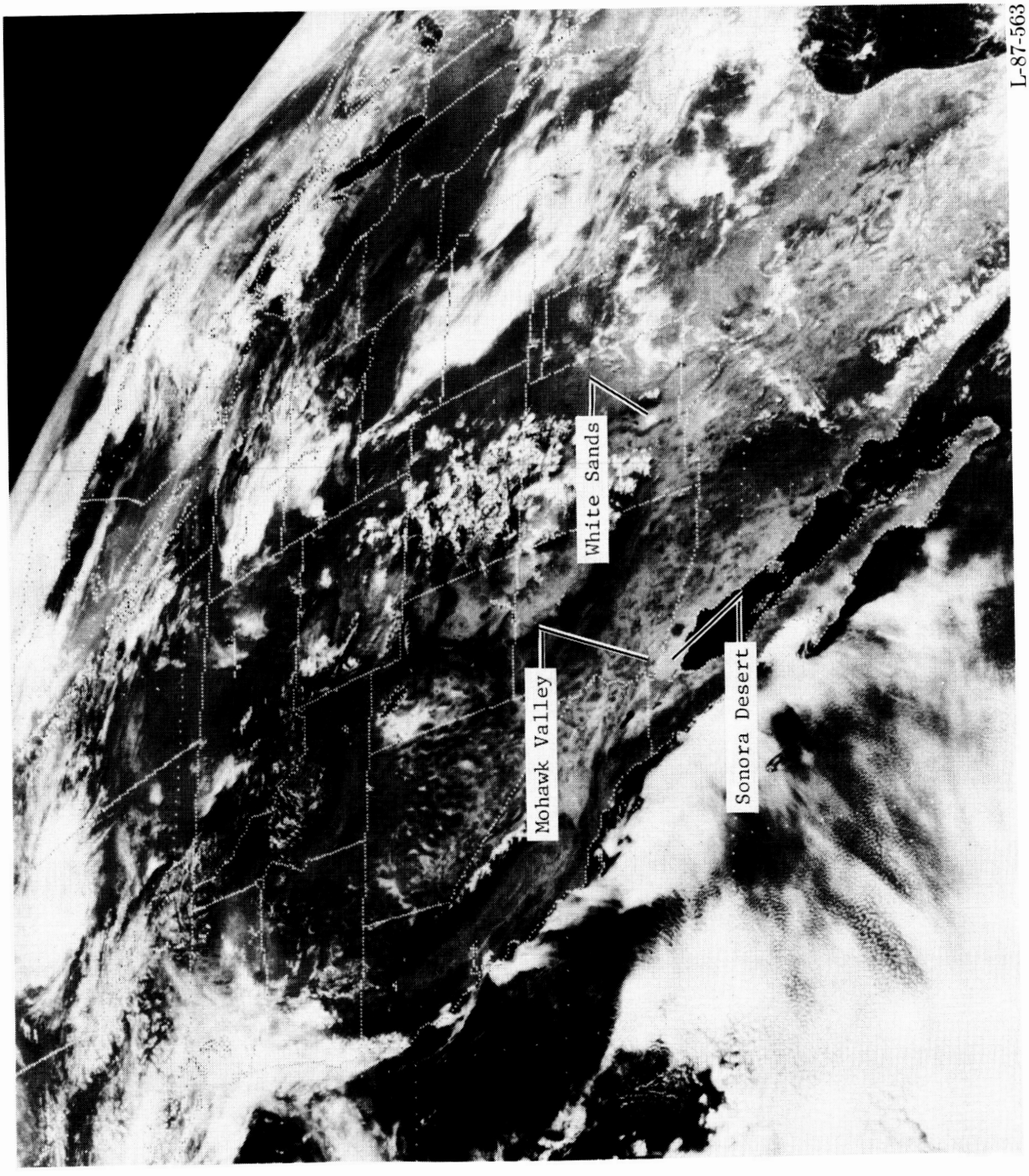

L-87-563

Figure 1. Satellite view of test sites.

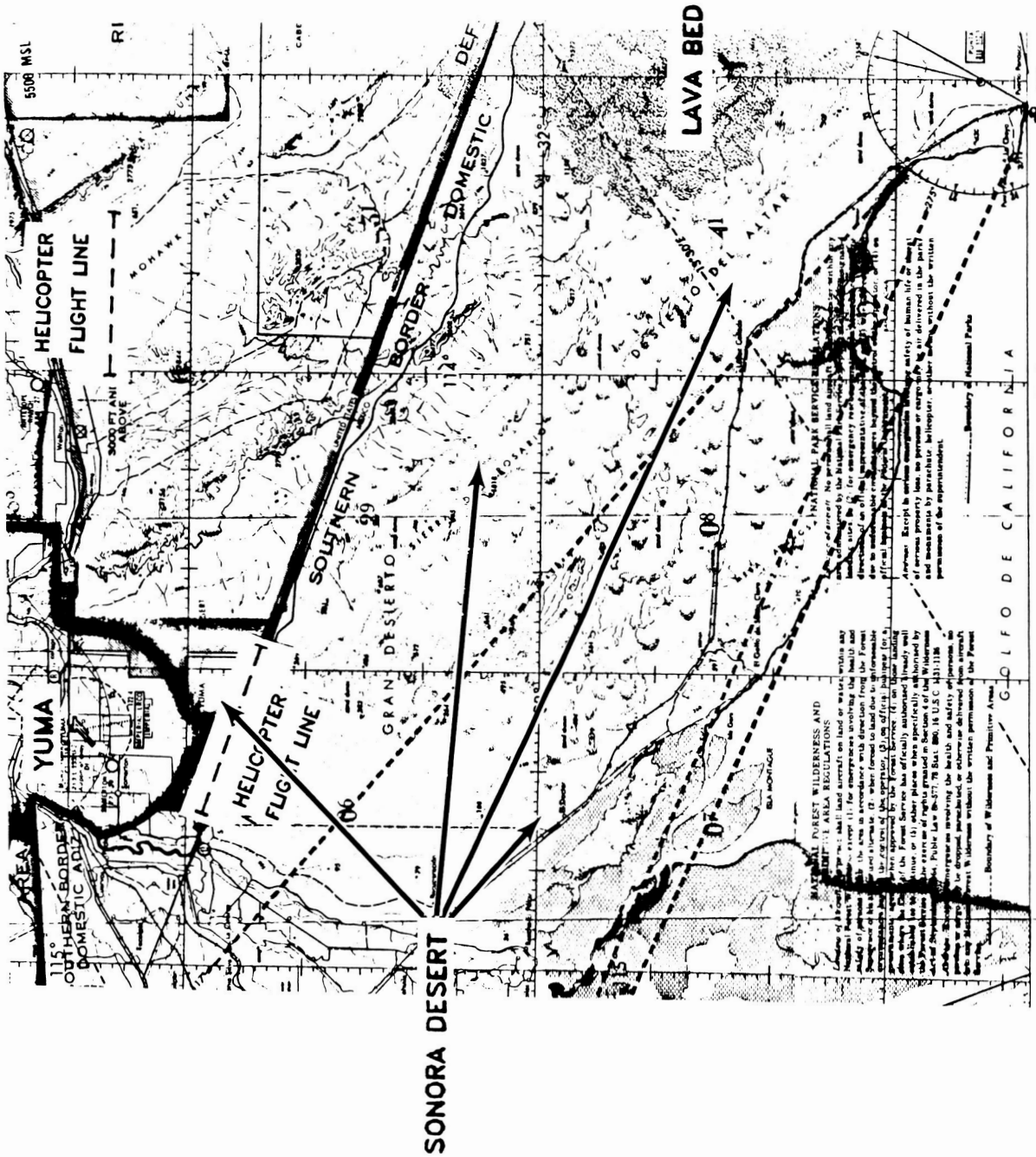

Figure 2. Helicopter flight locations on Phoenix Aeronautical Chart.

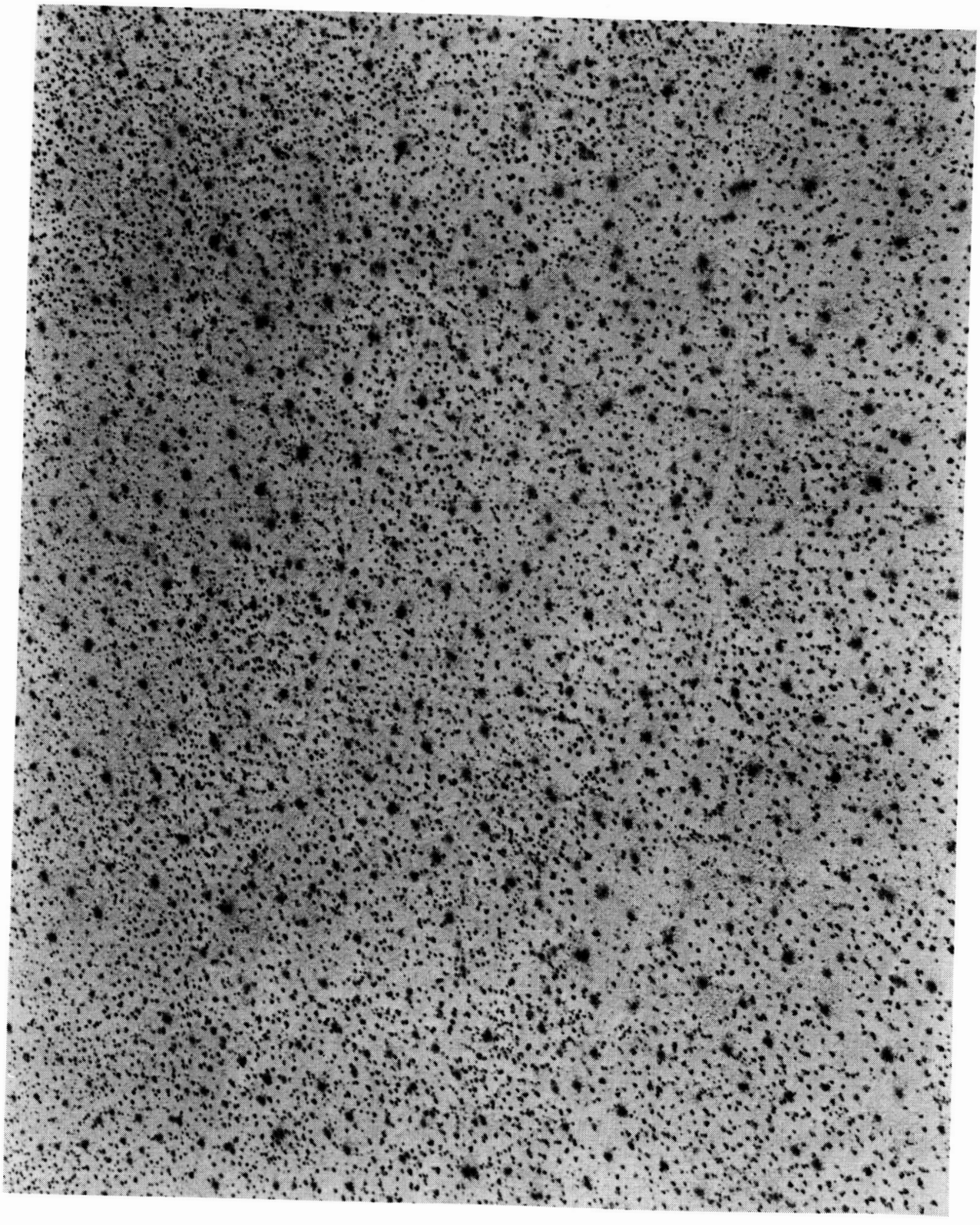

L-87-564

Figure 3. Nadir-view of Sonora Desert.

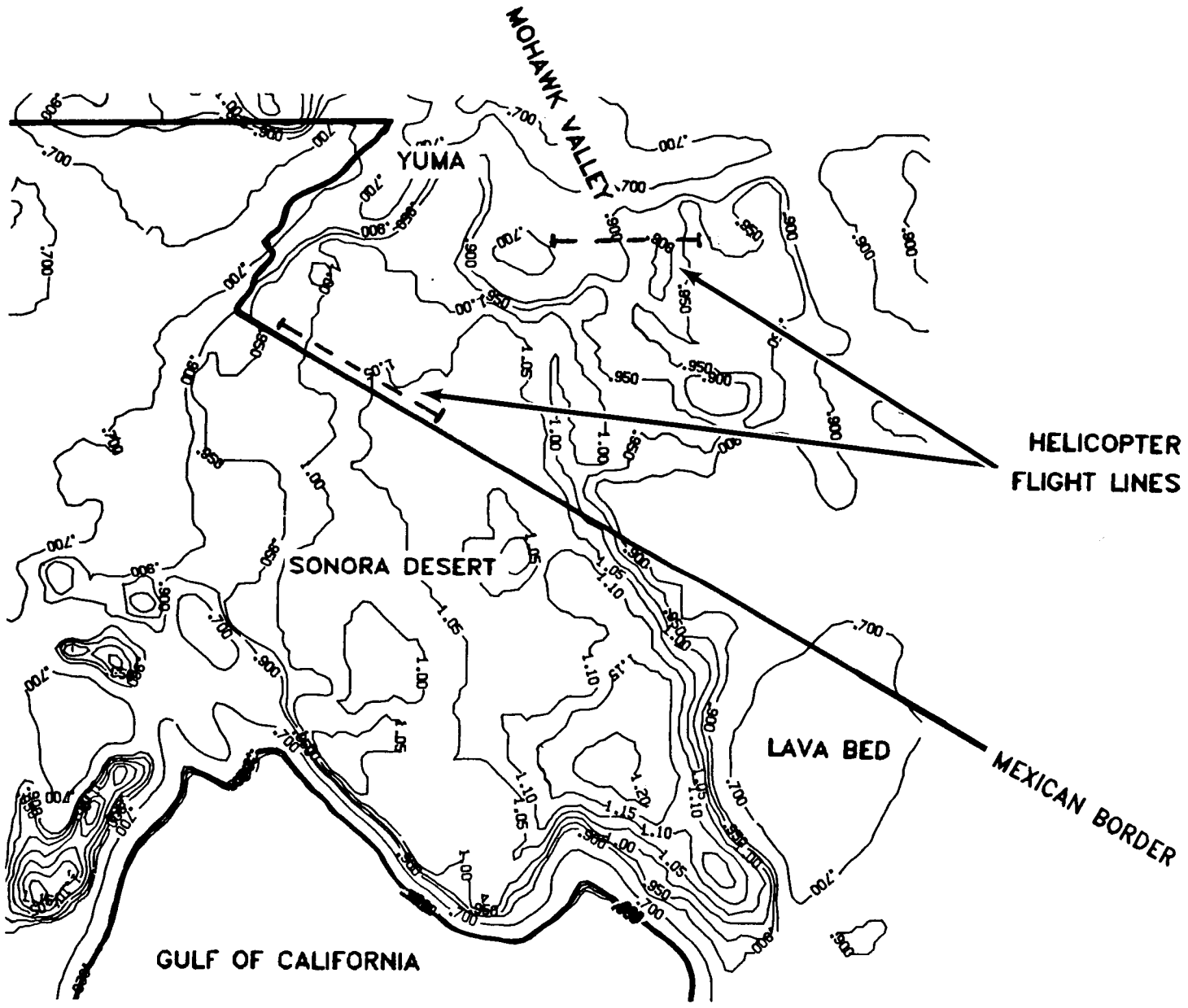

(a) AVHRR band 1 (0.57–0.70 μm) on May 13, 1985.

Figure 4. Variation of top-of-atmosphere albedo relative to Sonora Desert flight-line average value.

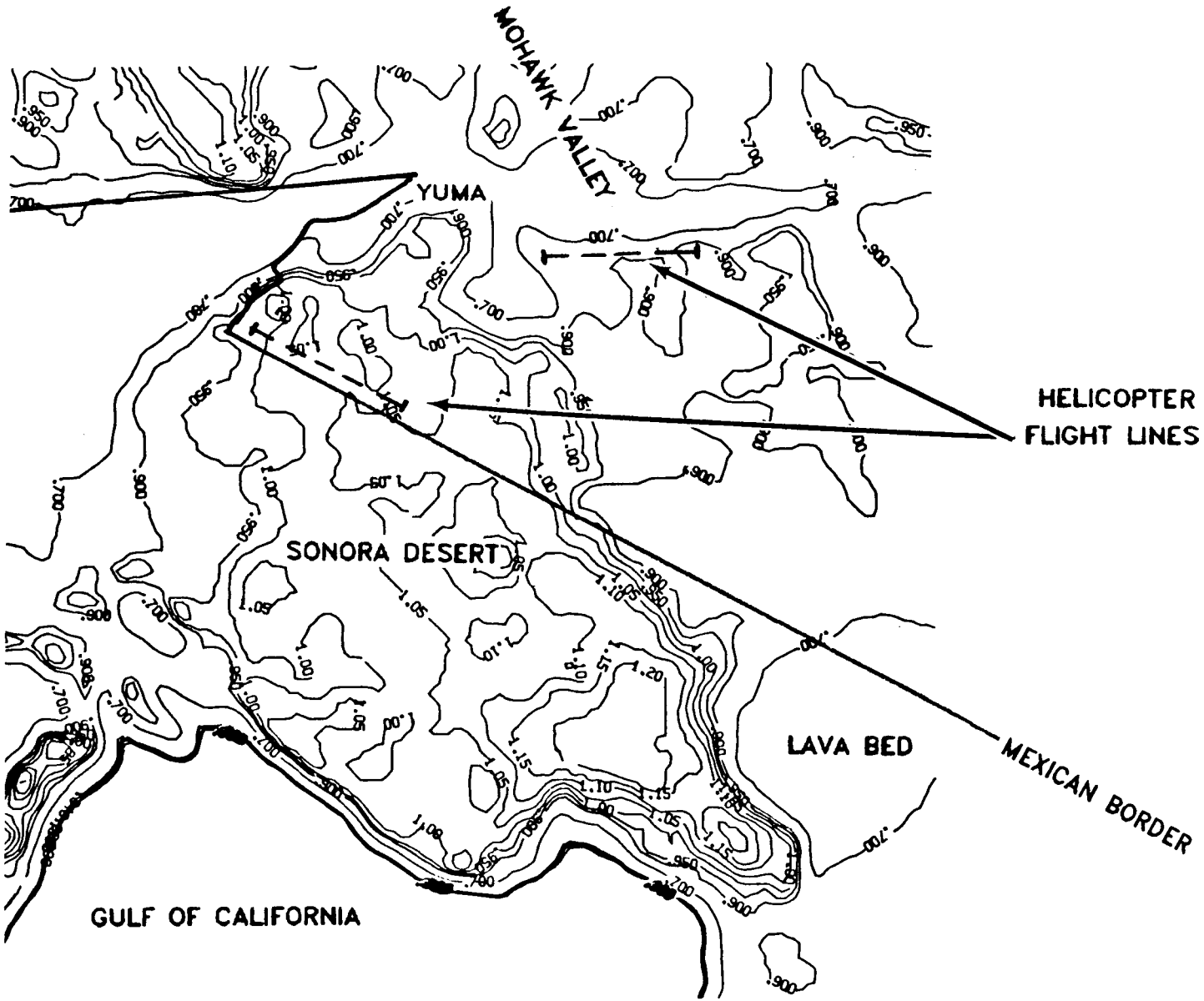

(b) AVHRR band 1 (0.57–0.70 μm) on May 14, 1985.

Figure 4. Concluded.

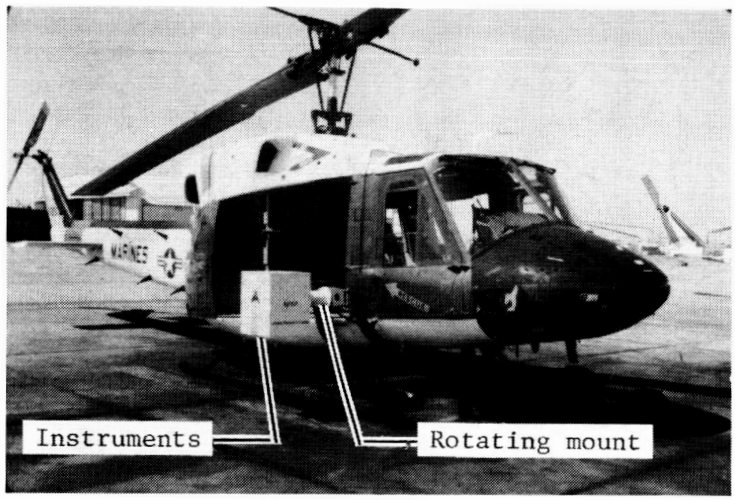

(a) External configuration.

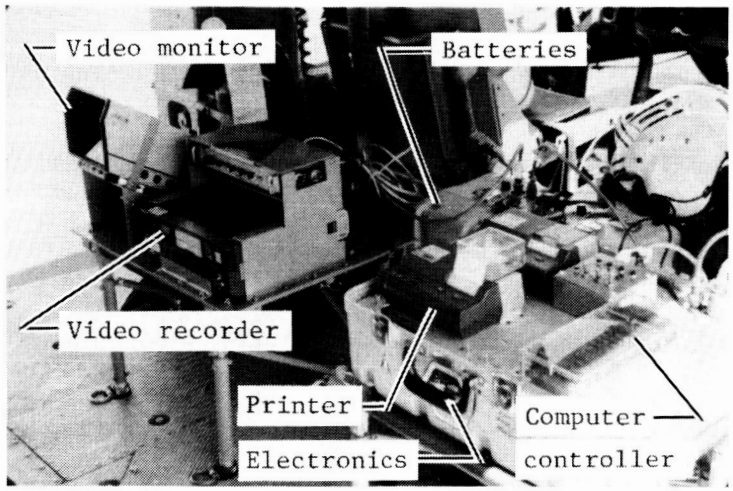

(b) Internal configuration.

L-87-565

Figure 5. Surface reflectance instrumentation.

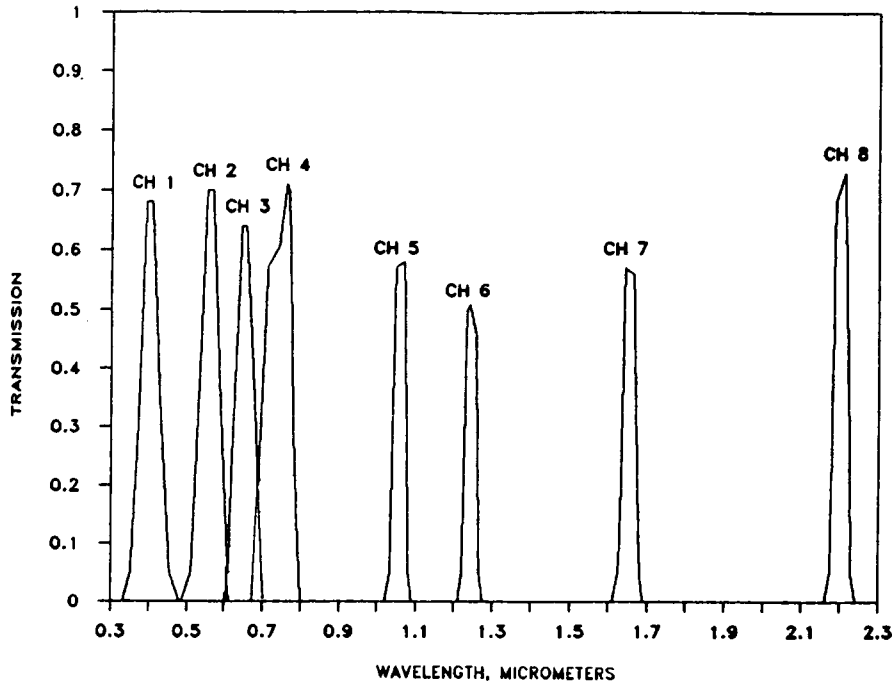

(a) Instrument filters.

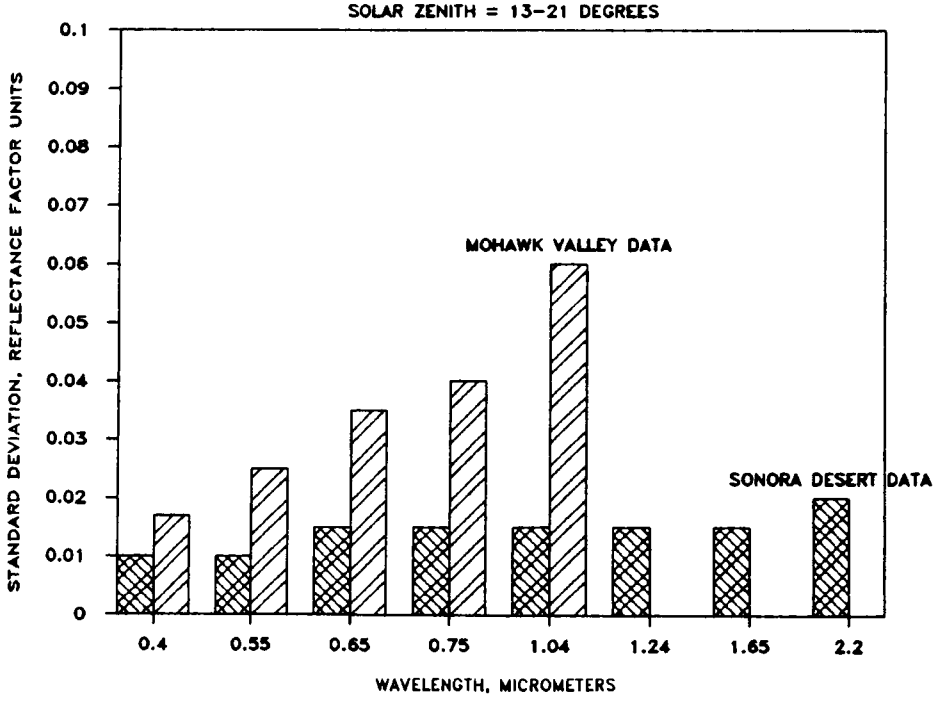

(b) Estimated uncertainties. Solar zenith angle, 13°–21°.

Figure 6. Instrument wavelengths and accuracies.

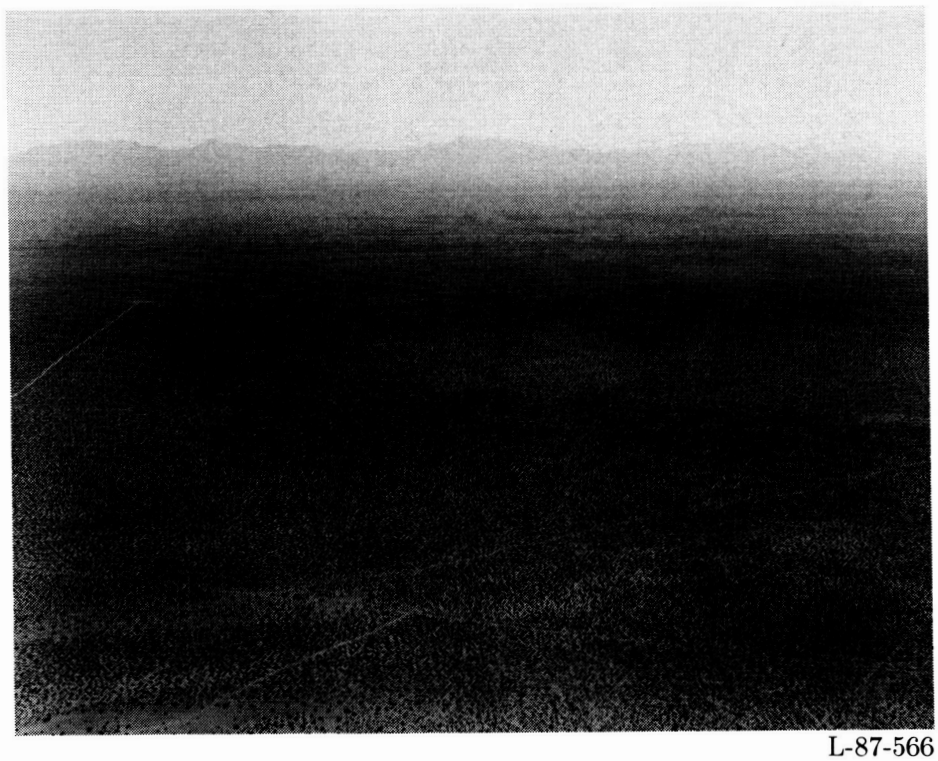

L-87-566

(a) Sonora Desert.

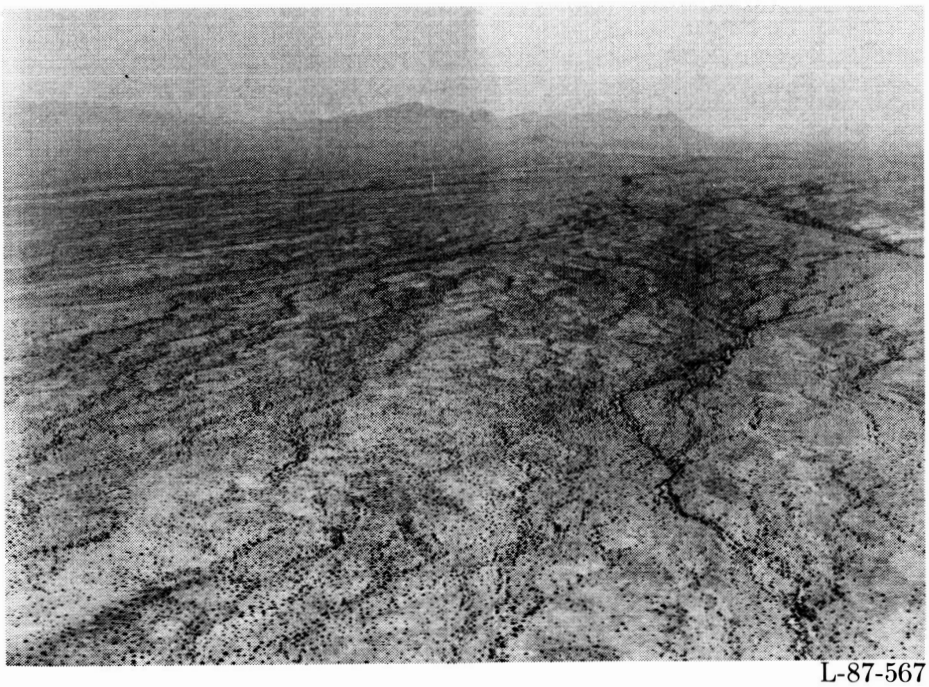

L-87-567

(b) Mohawk Valley.

Figure 7. Photographs of Sonora Desert and Mohawk Valley.

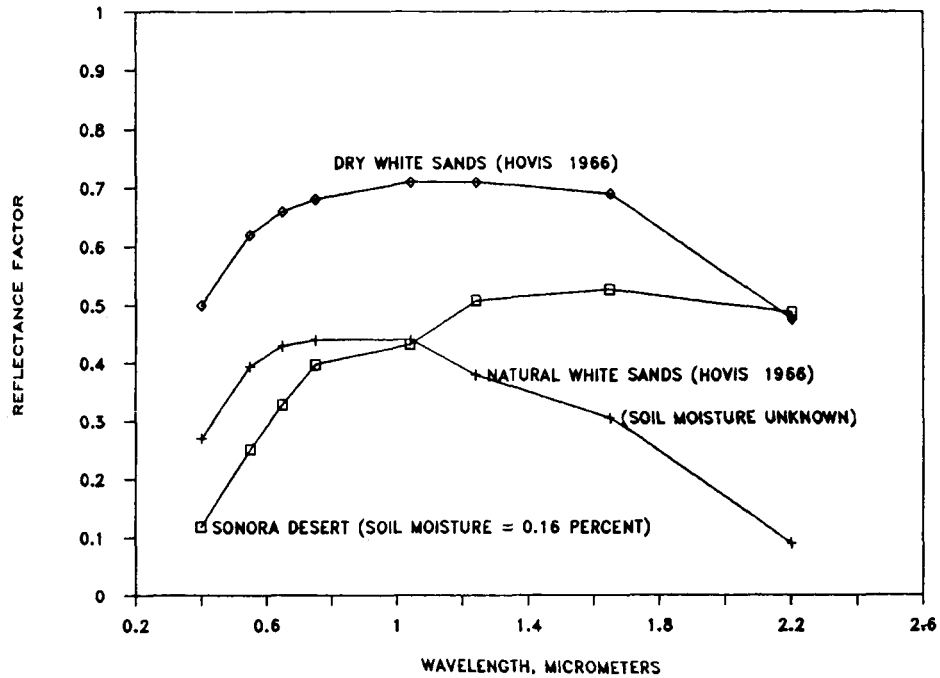

(a) Nadir desert reflectance.

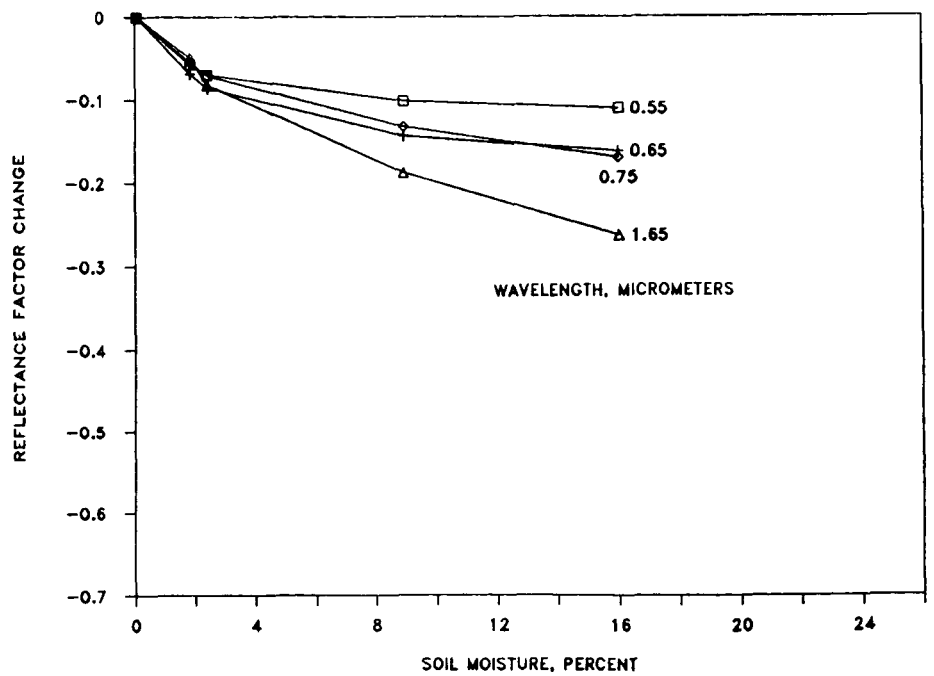

(b) Loss from soil moisture for Sonora Desert bare sand.

Figure 8. Nadir reflectance and soil moisture effects.

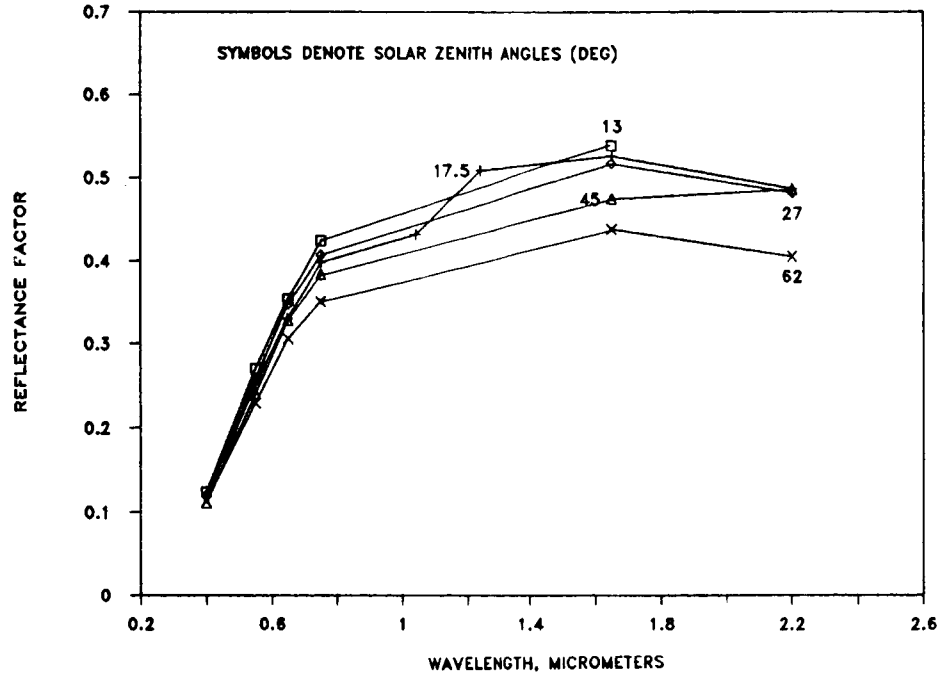

(a) Wavelength effects.

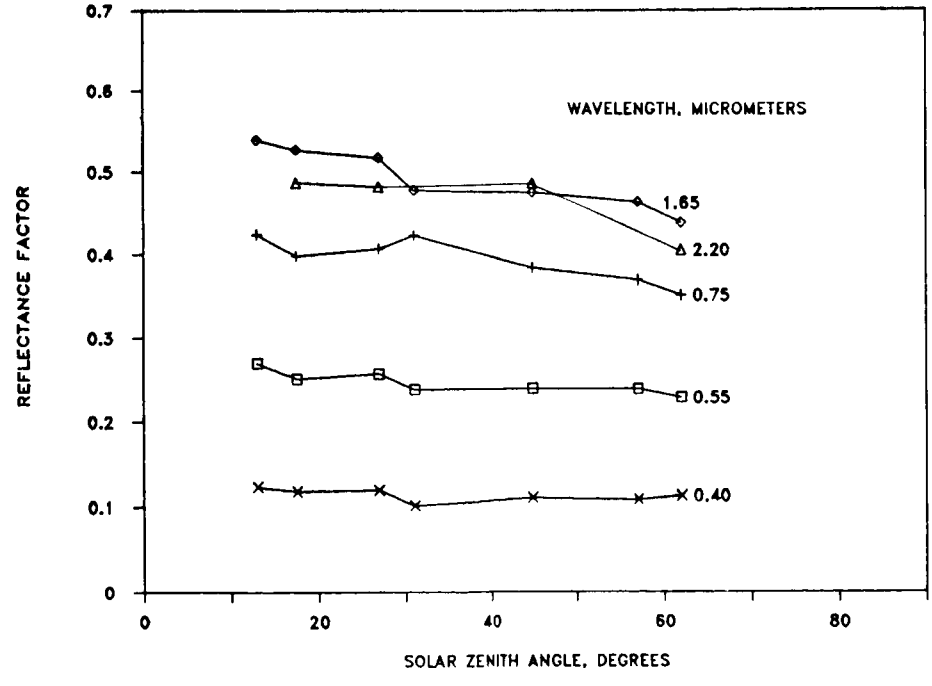

(b) Solar angle effects.

Figure 9. Solar angle effects on nadir Sonora reflectance.

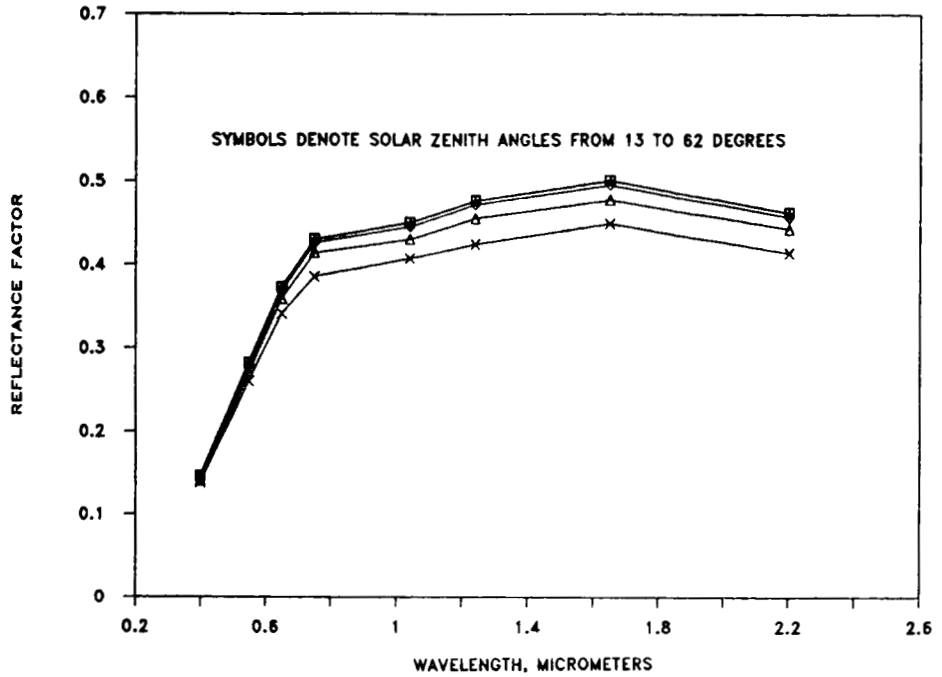

(a) Wavelength effects.

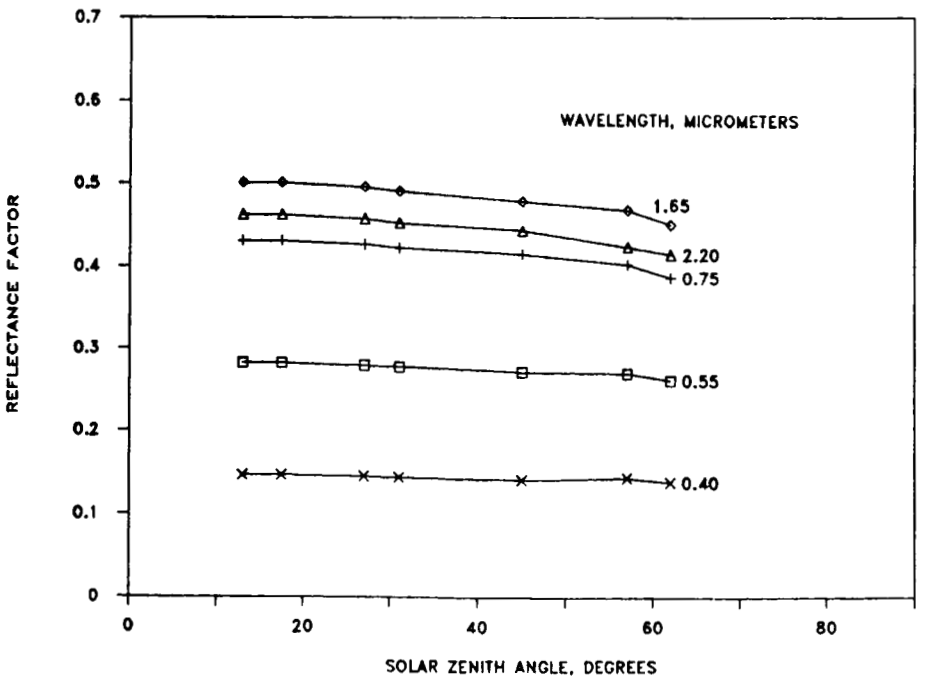

(b) Solar angle effects.

Figure 10. Solar angle effects on Sonora bare sand nadir reflectance (secondary target).

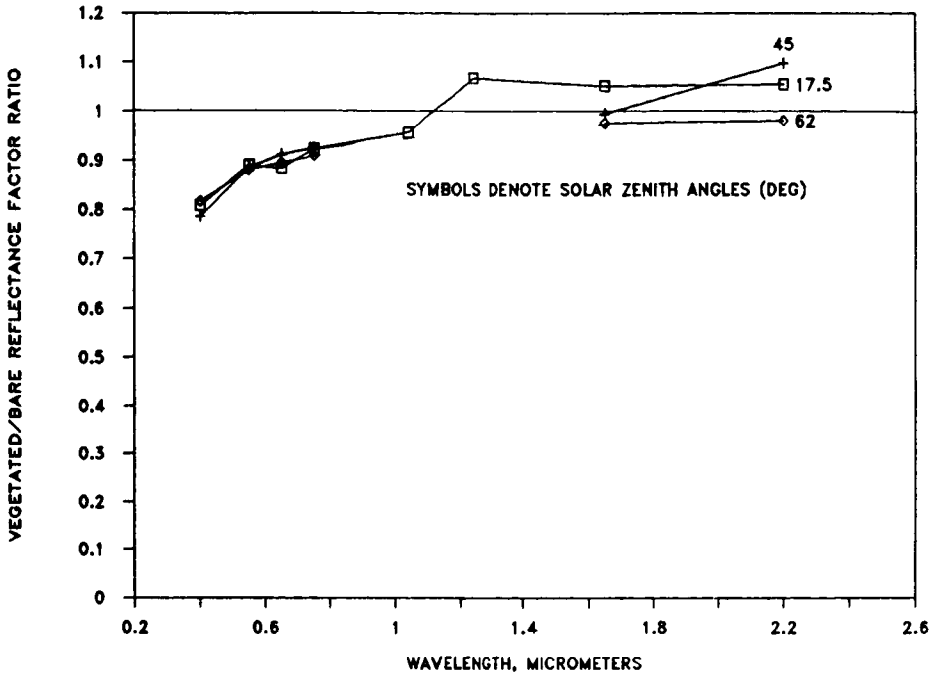

(a) Vegetation effect on Sonora reflectance.

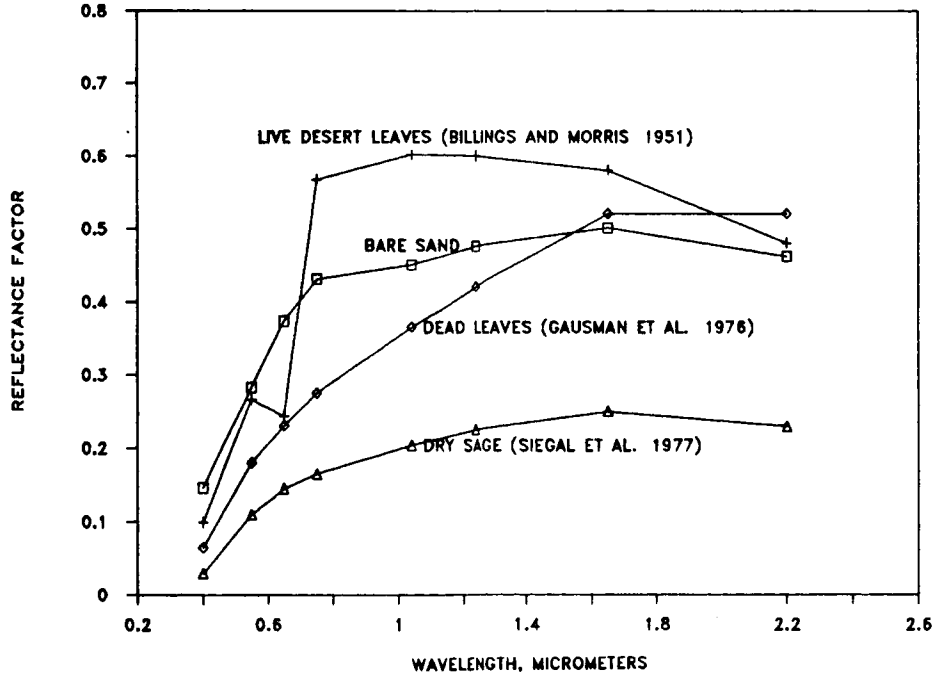

(b) Vegetation and bare sand reflectance.

Figure 11. Comparison of vegetation and sand spectra. Nadir view.

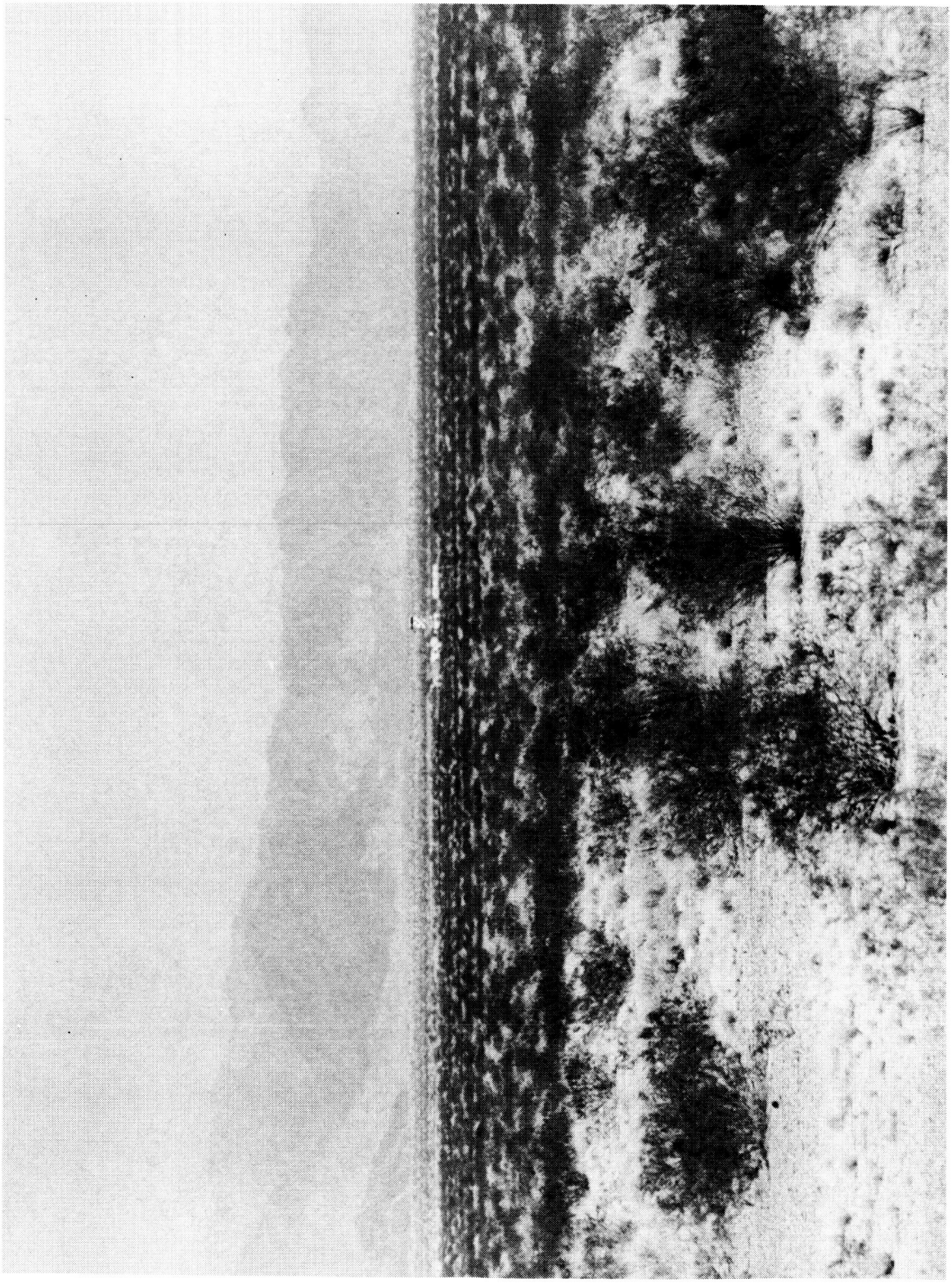

L-87-568

Figure 12. Sonora Desert vegetation.

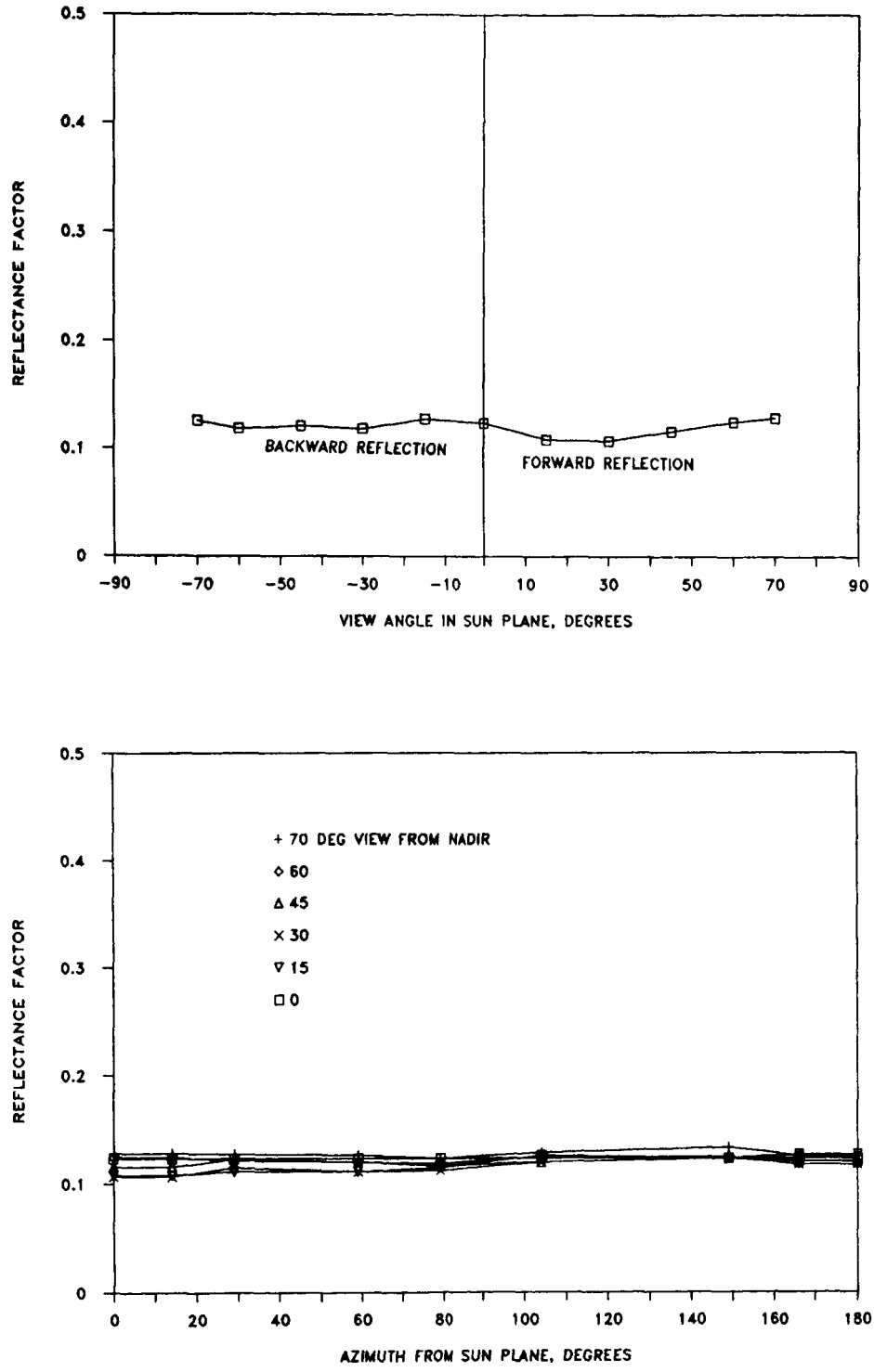

(a) Wavelength, 0.4 μm.

Figure 13. Bidirectional reflectance for solar zenith angle of 13°.

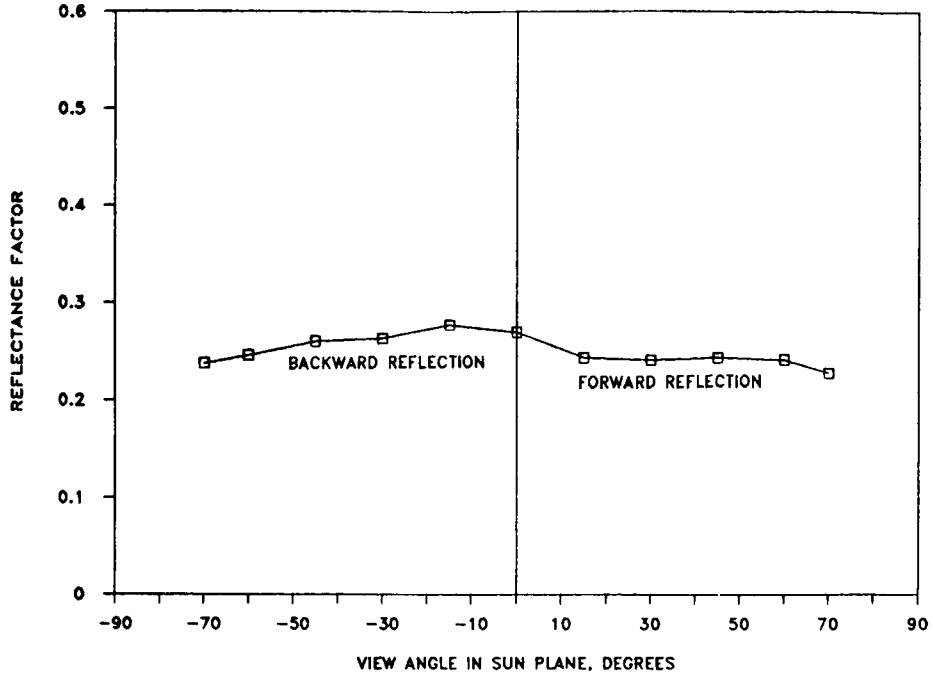

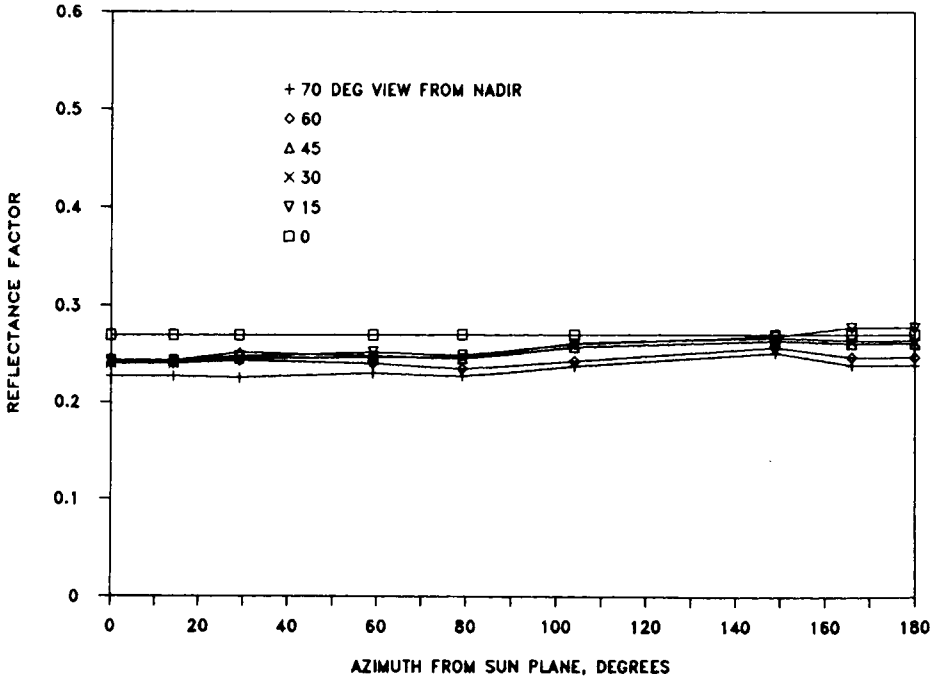

(b) Wavelength, 0.55 μm.

Figure 13. Continued.

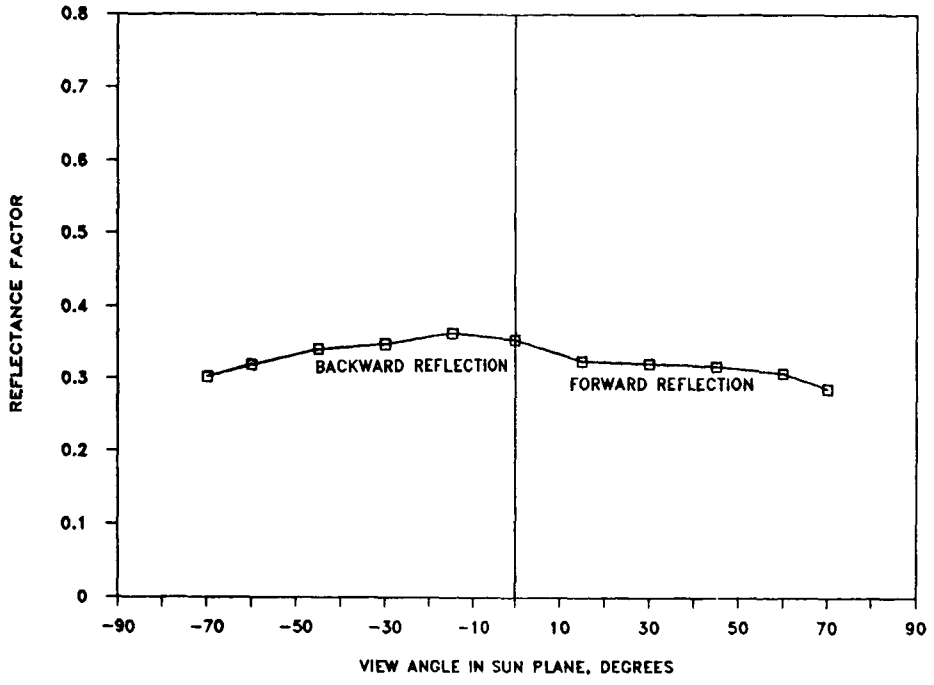

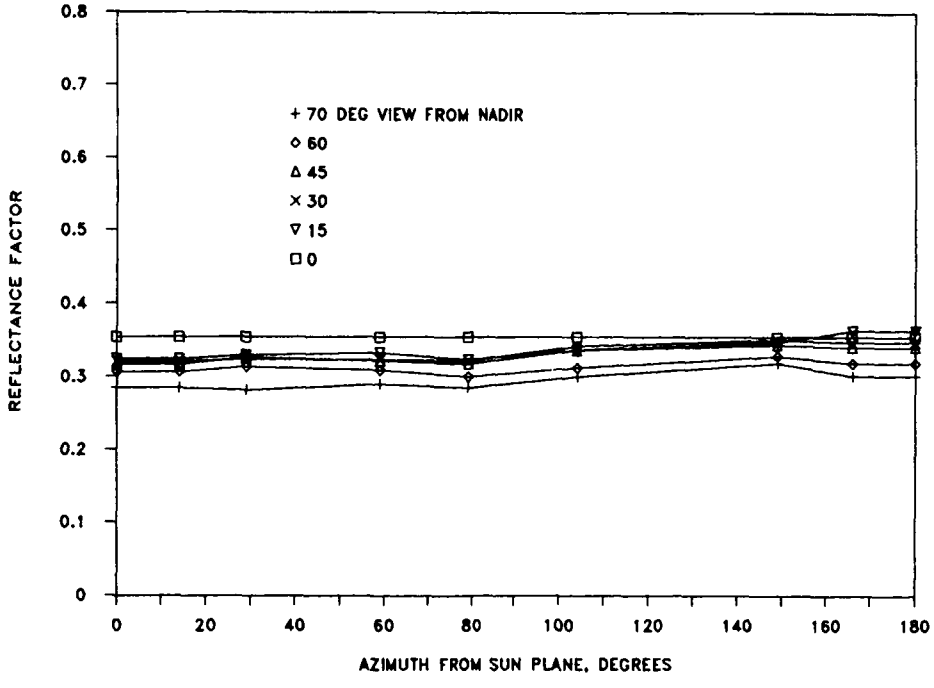

(c) Wavelength, 0.65 μm.

Figure 13. Continued.

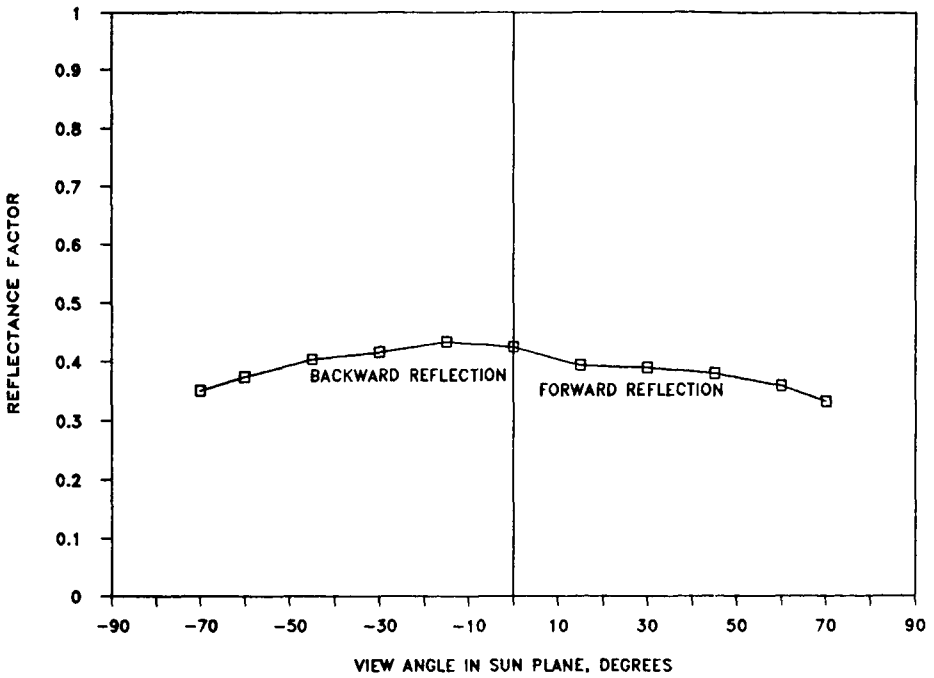

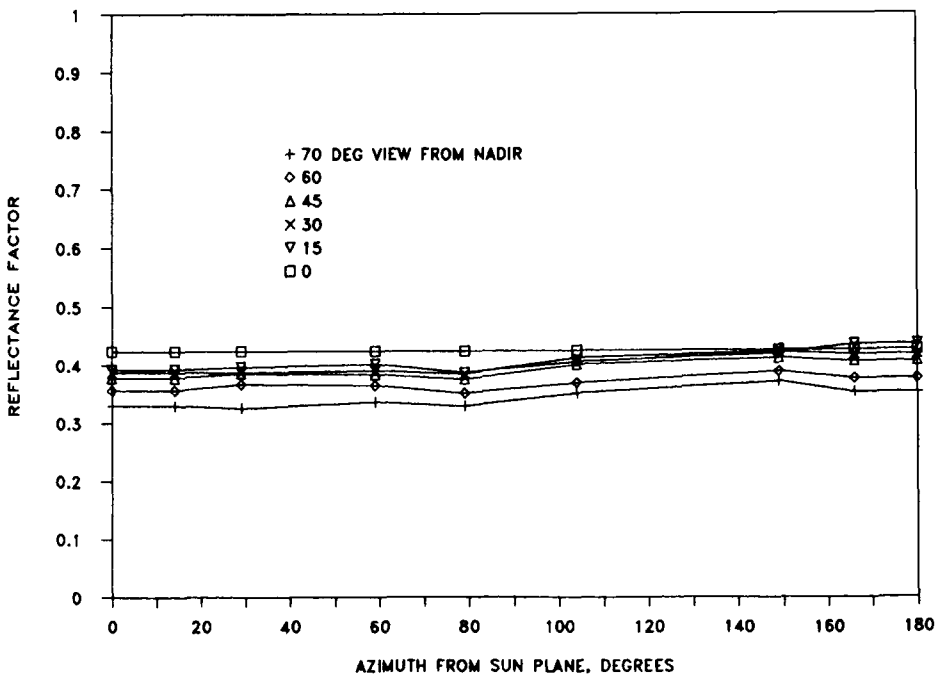

(d) Wavelength, 0.75 μm.

Figure 13. Continued.

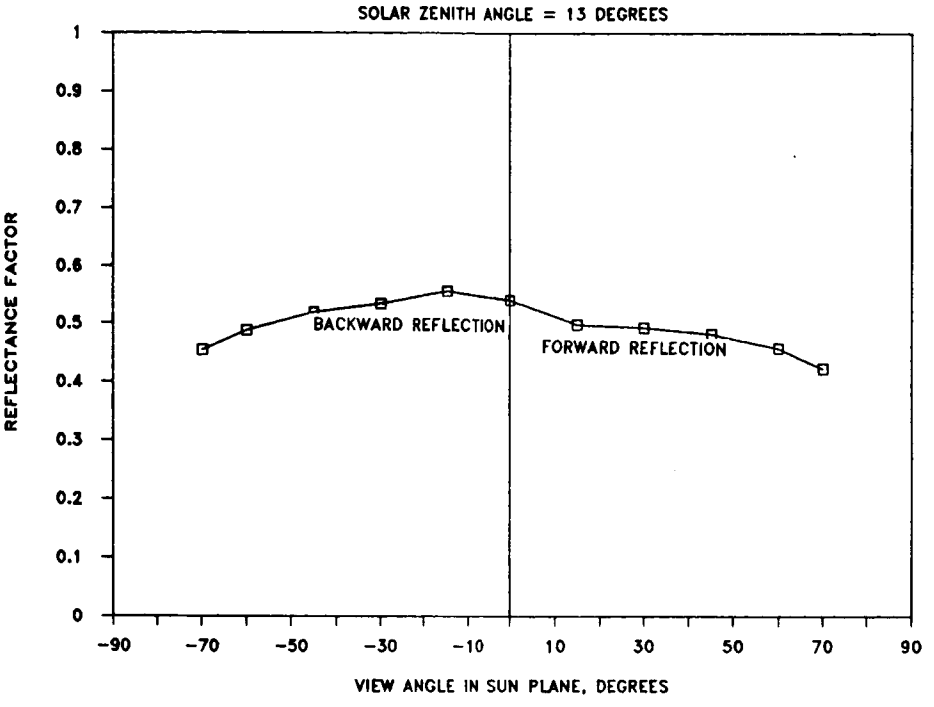

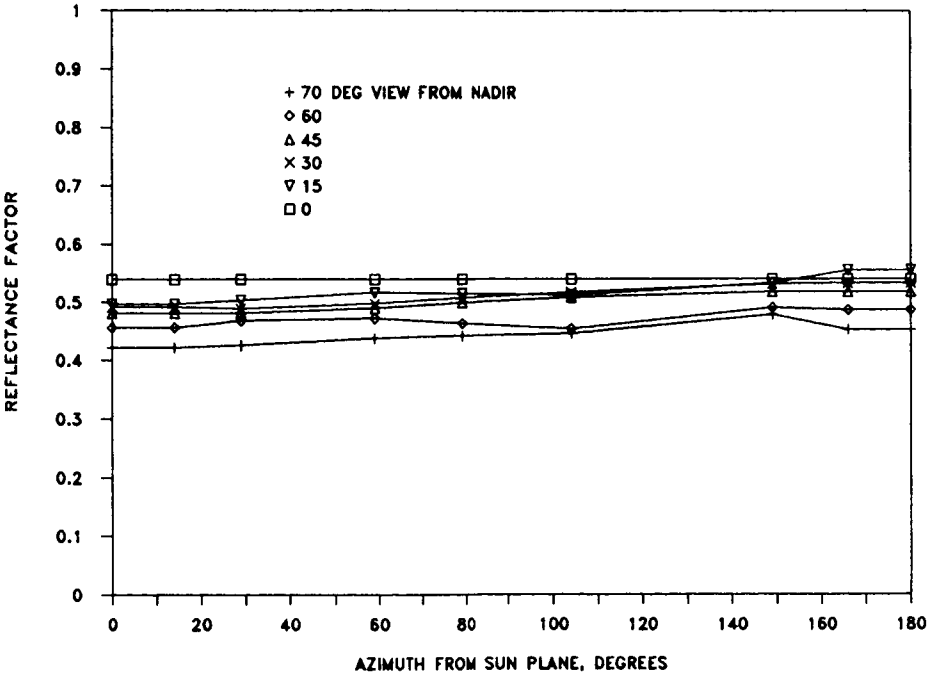

(e) Wavelength, 1.65 μm.

Figure 13. Concluded.

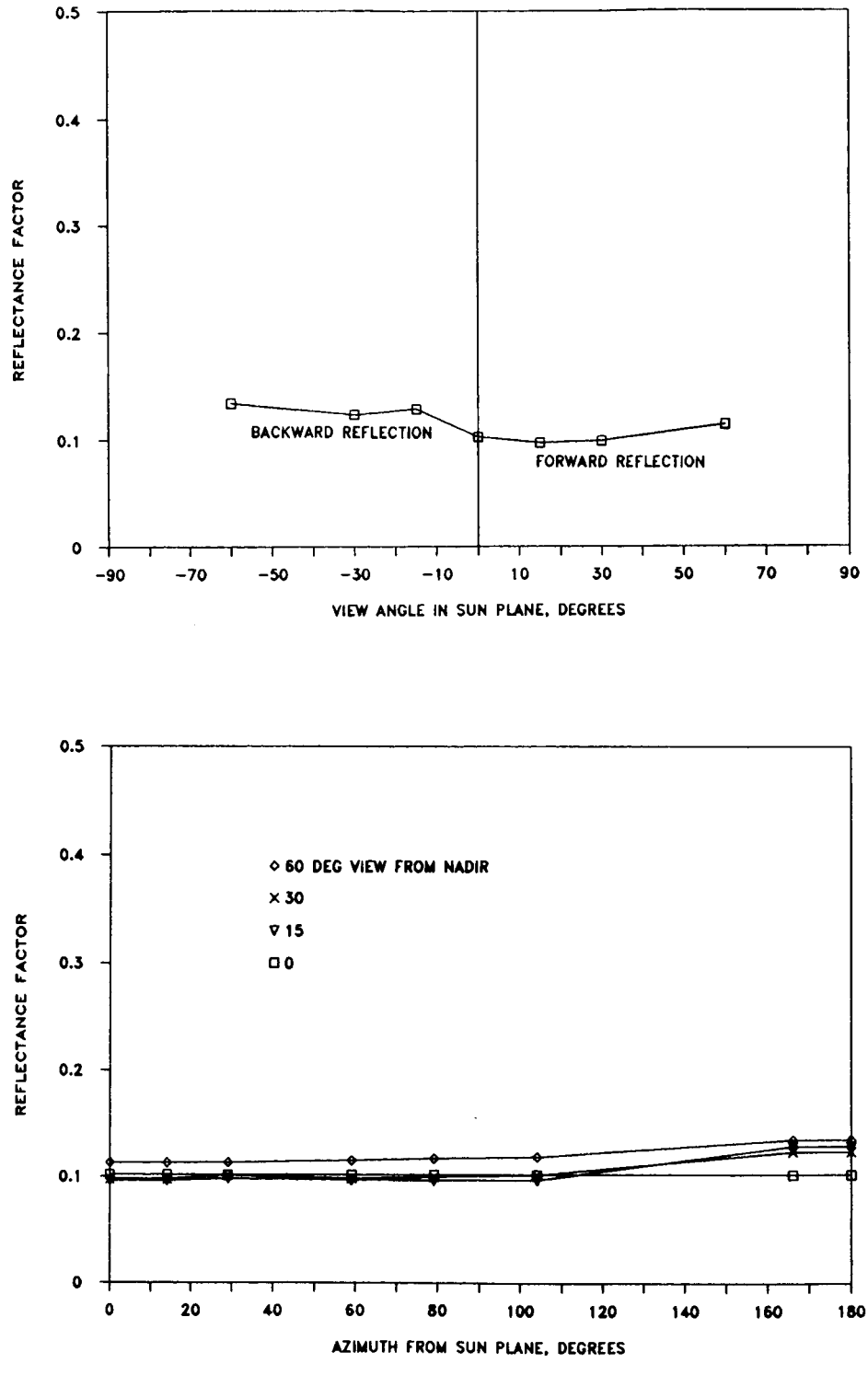

(a) Wavelength, 0.4 μm.

Figure 14. Bidirectional reflectance for solar zenith angle of 31°.

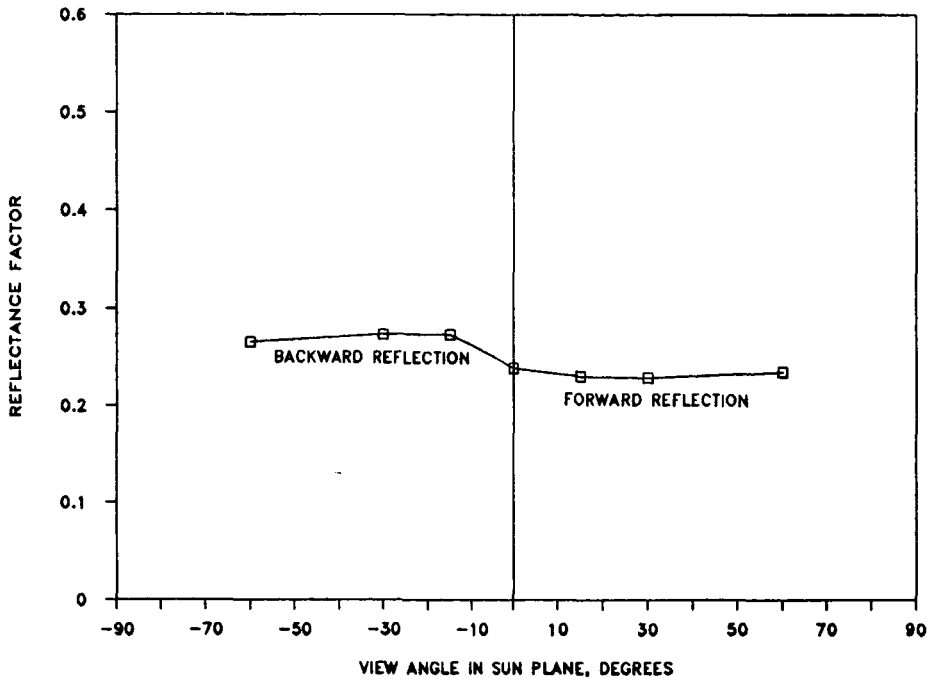

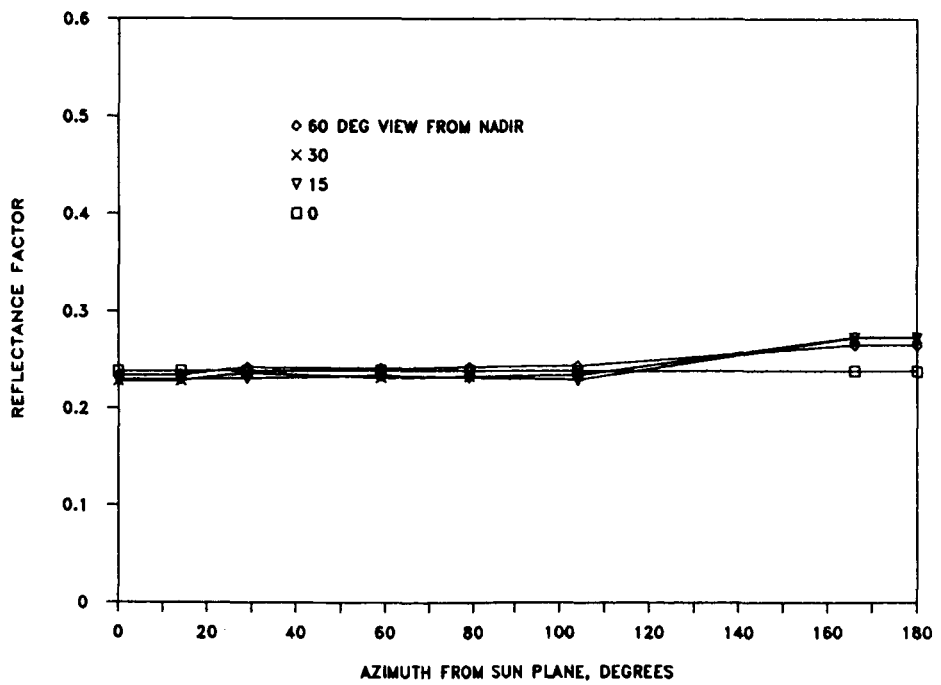

(b) Wavelength, 0.55 μm.

Figure 14. Continued.

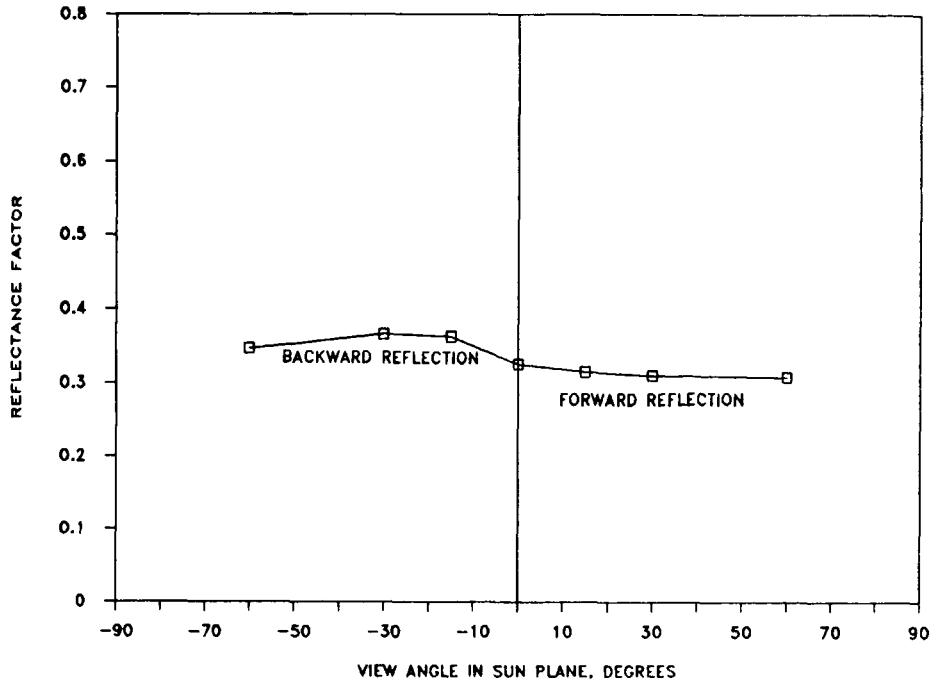

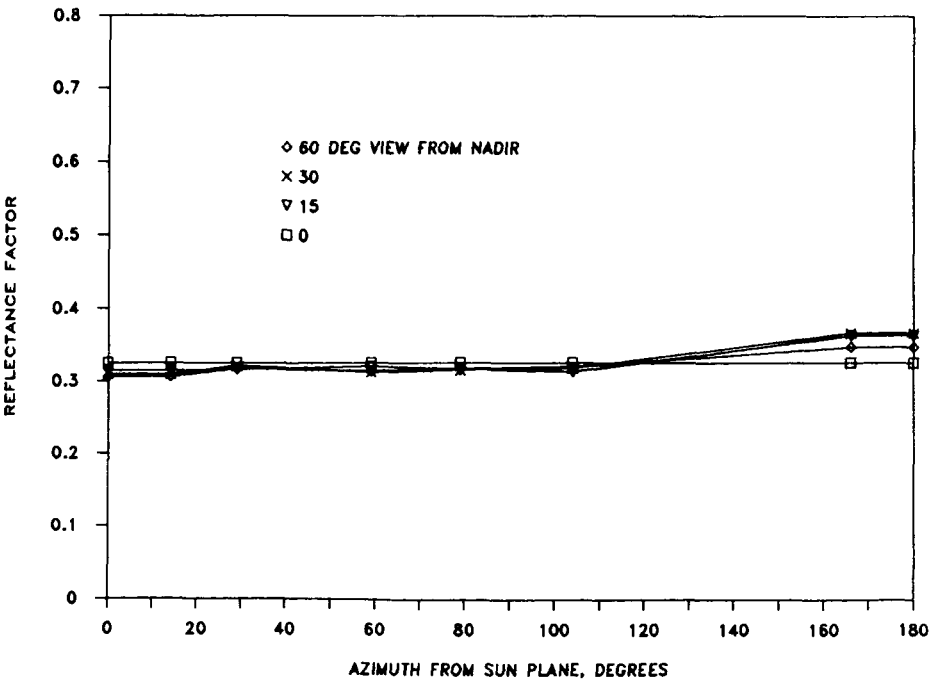

(c) Wavelength, 0.65 μm.

Figure 14. Continued.

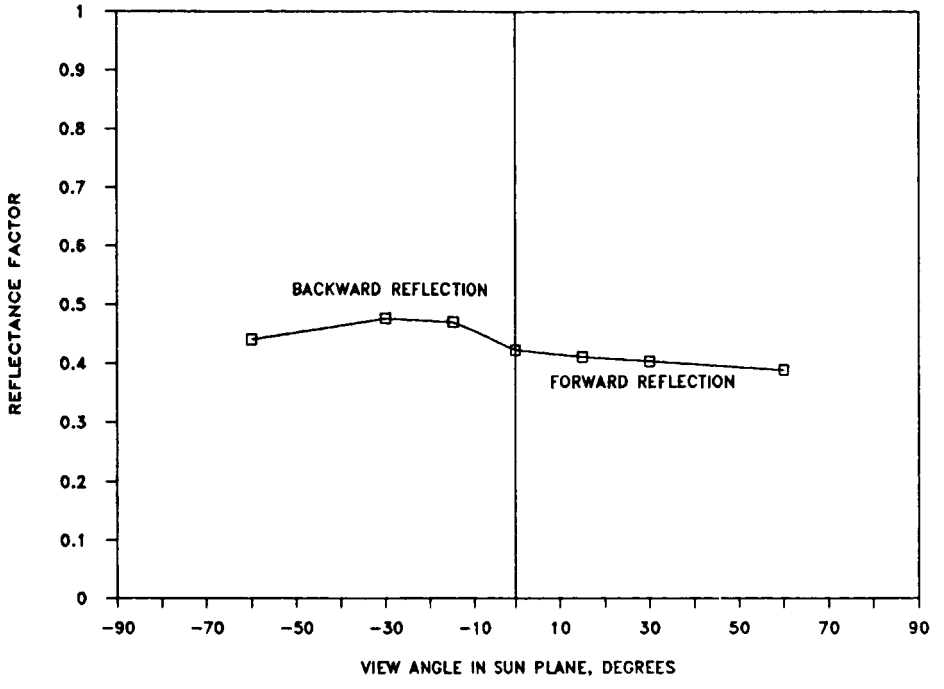

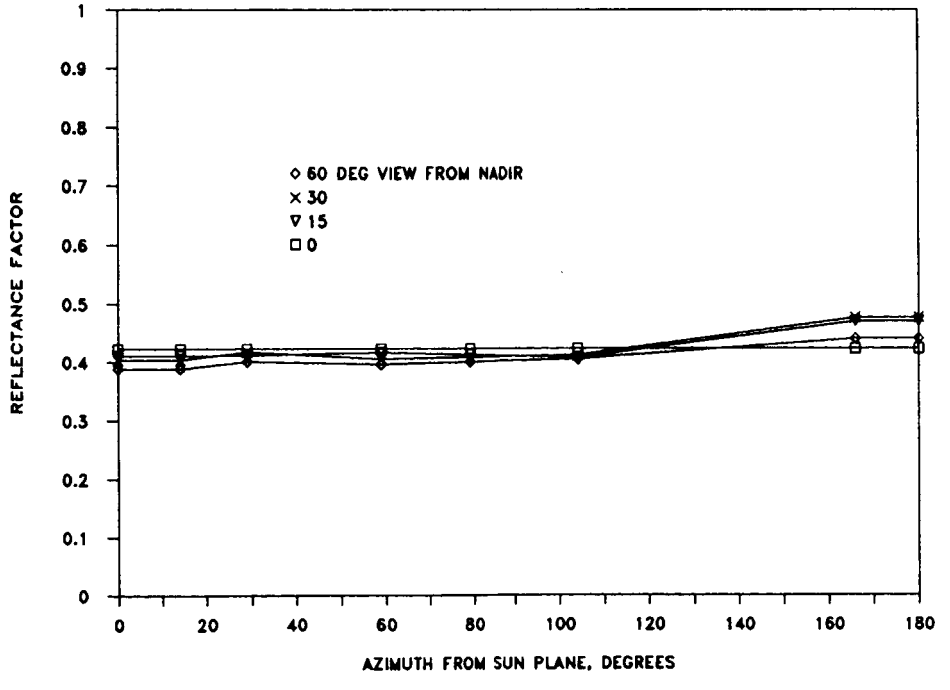

(d) Wavelength, 0.75 μm.

Figure 14. Continued.

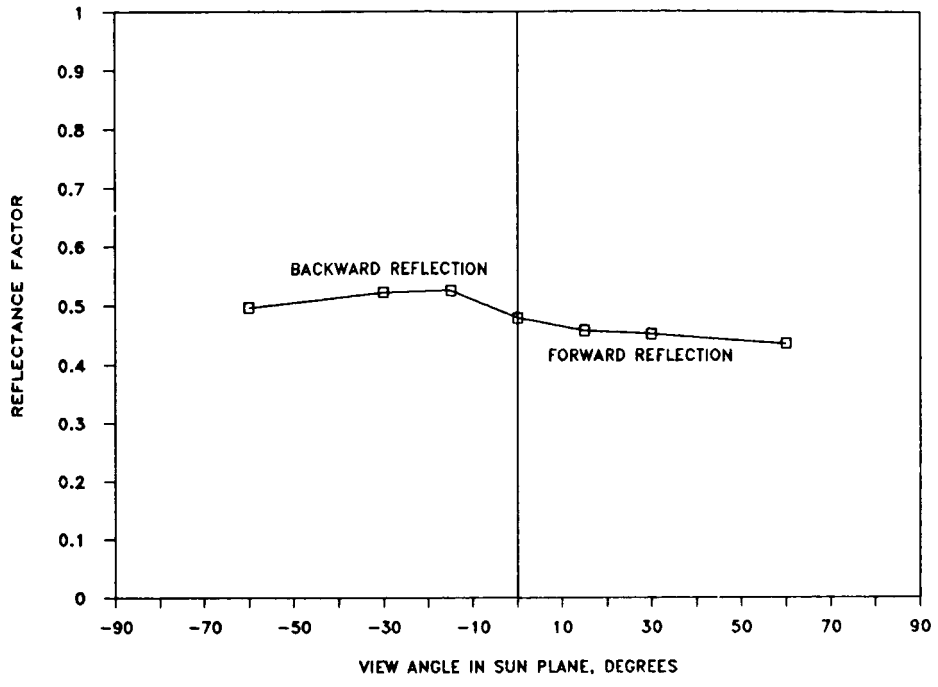

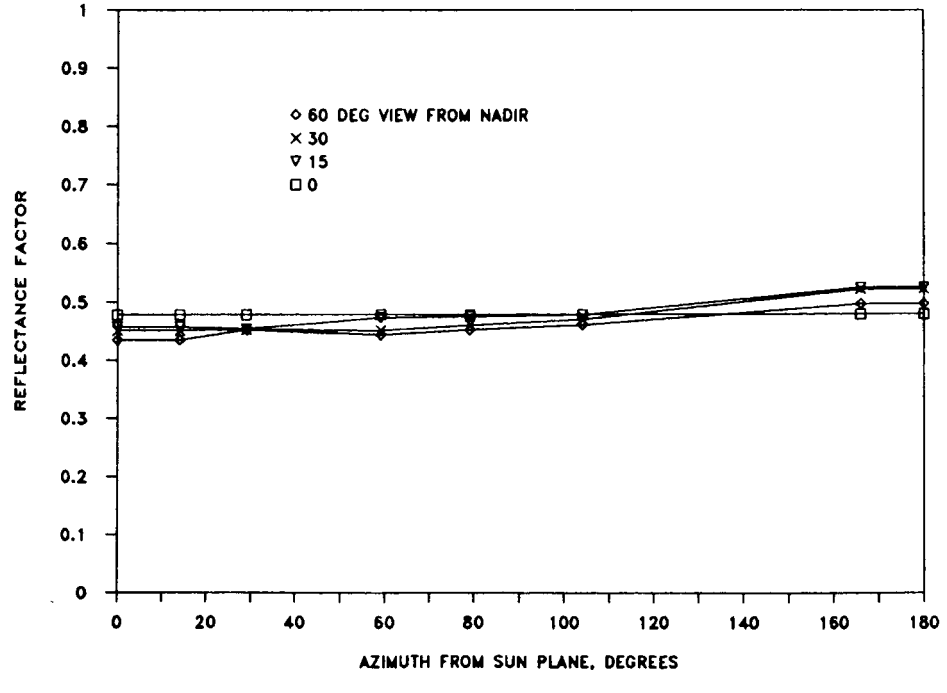

(e) Wavelength, 1.65 μm.

Figure 14. Concluded.

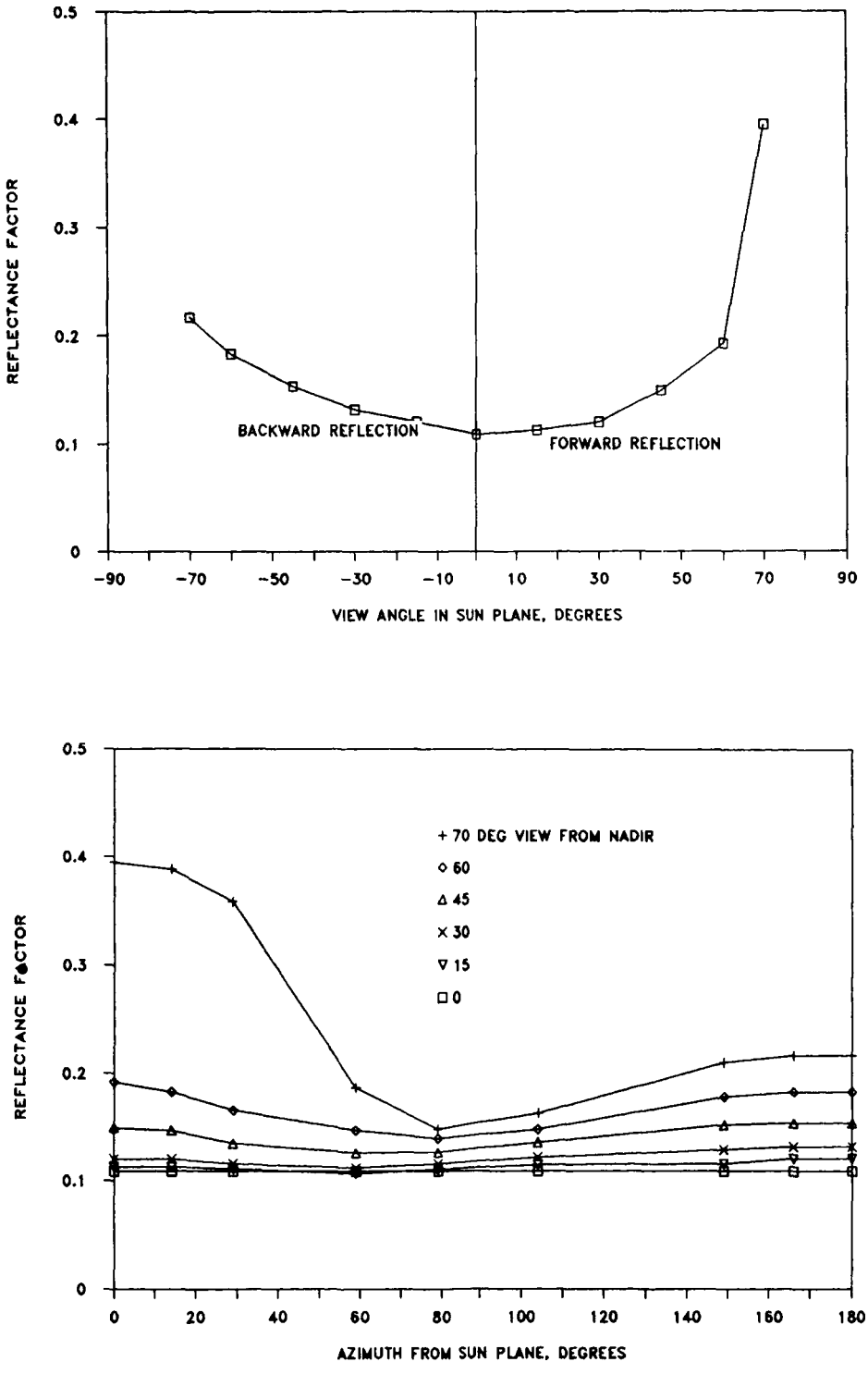

(a) Wavelength, 0.4 μm.

Figure 15. Bidirectional reflectance for solar zenith angle of 57°.

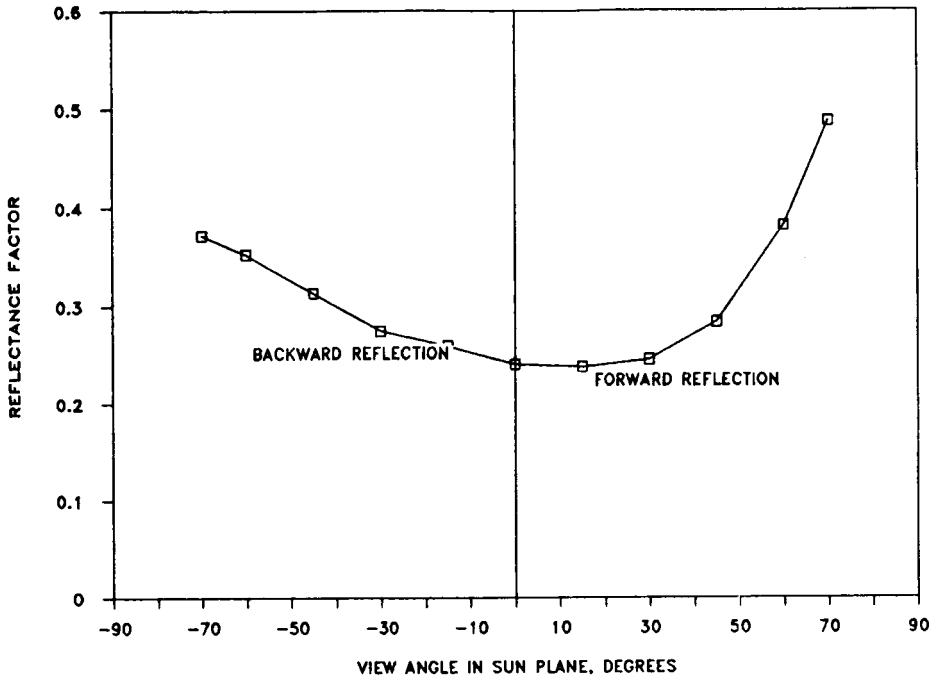

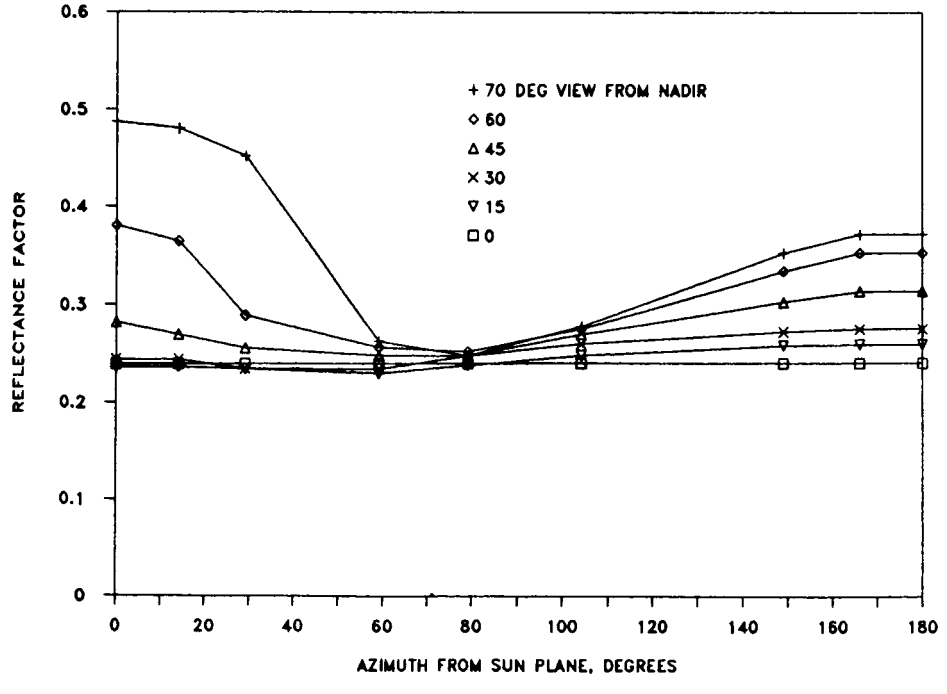

(b) Wavelength, 0.55 μm.

Figure 15. Continued.

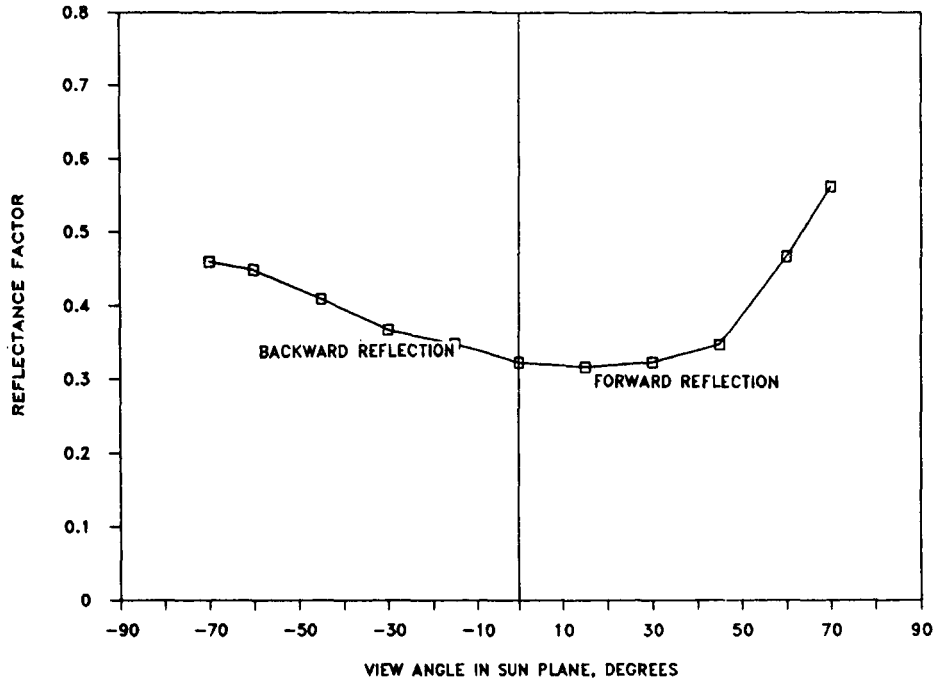

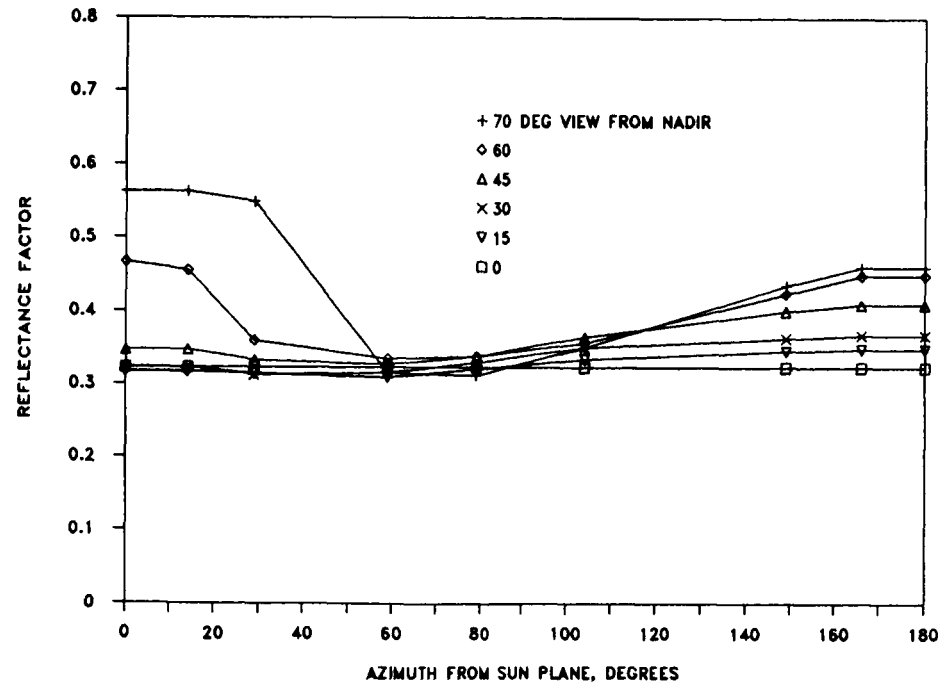

(c) Wavelength, 0.65 μm.

Figure 15. Continued.

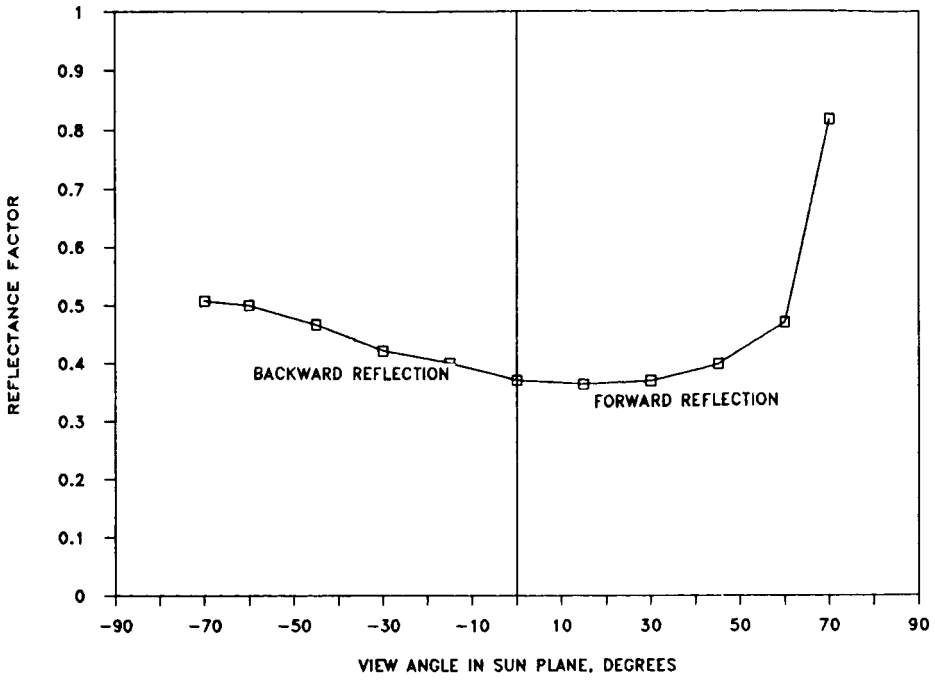

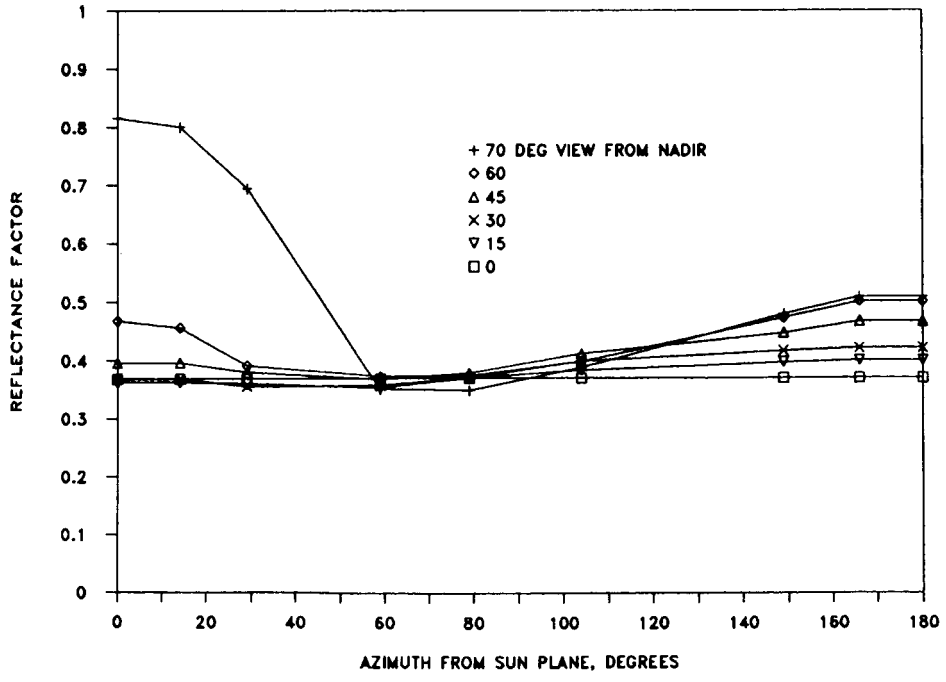

(d) Wavelength, 0.75 μm.

Figure 15. Continued.

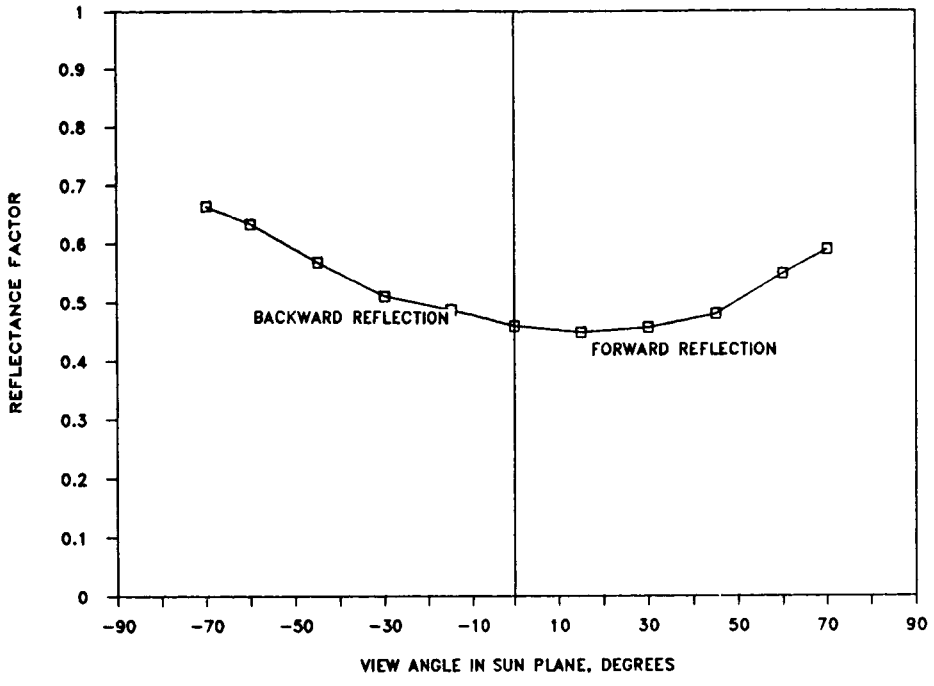

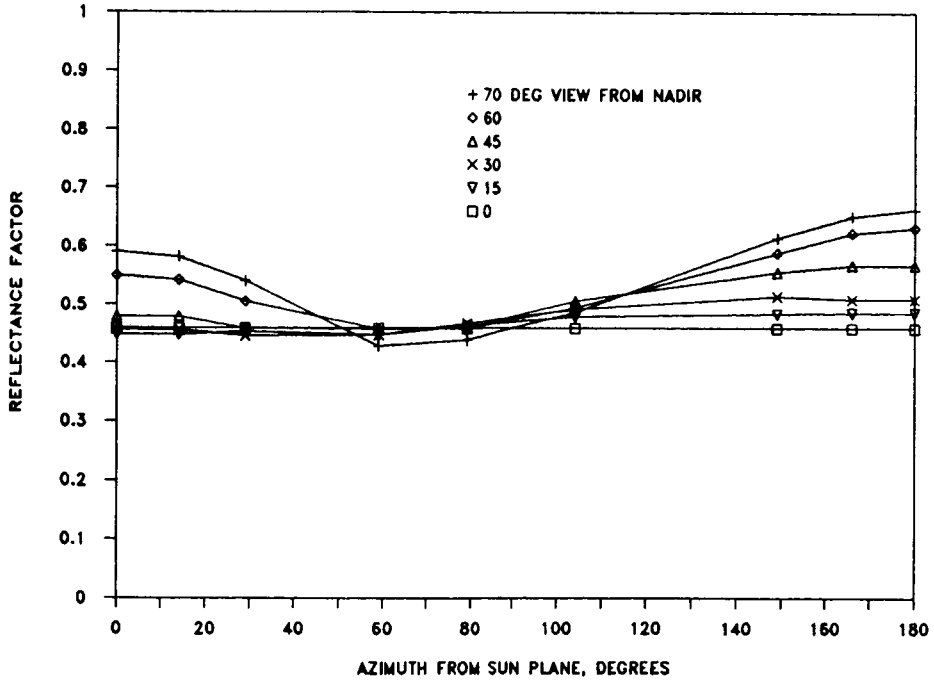

(e) Wavelength, 1.65 μm.

Figure 15. Concluded.

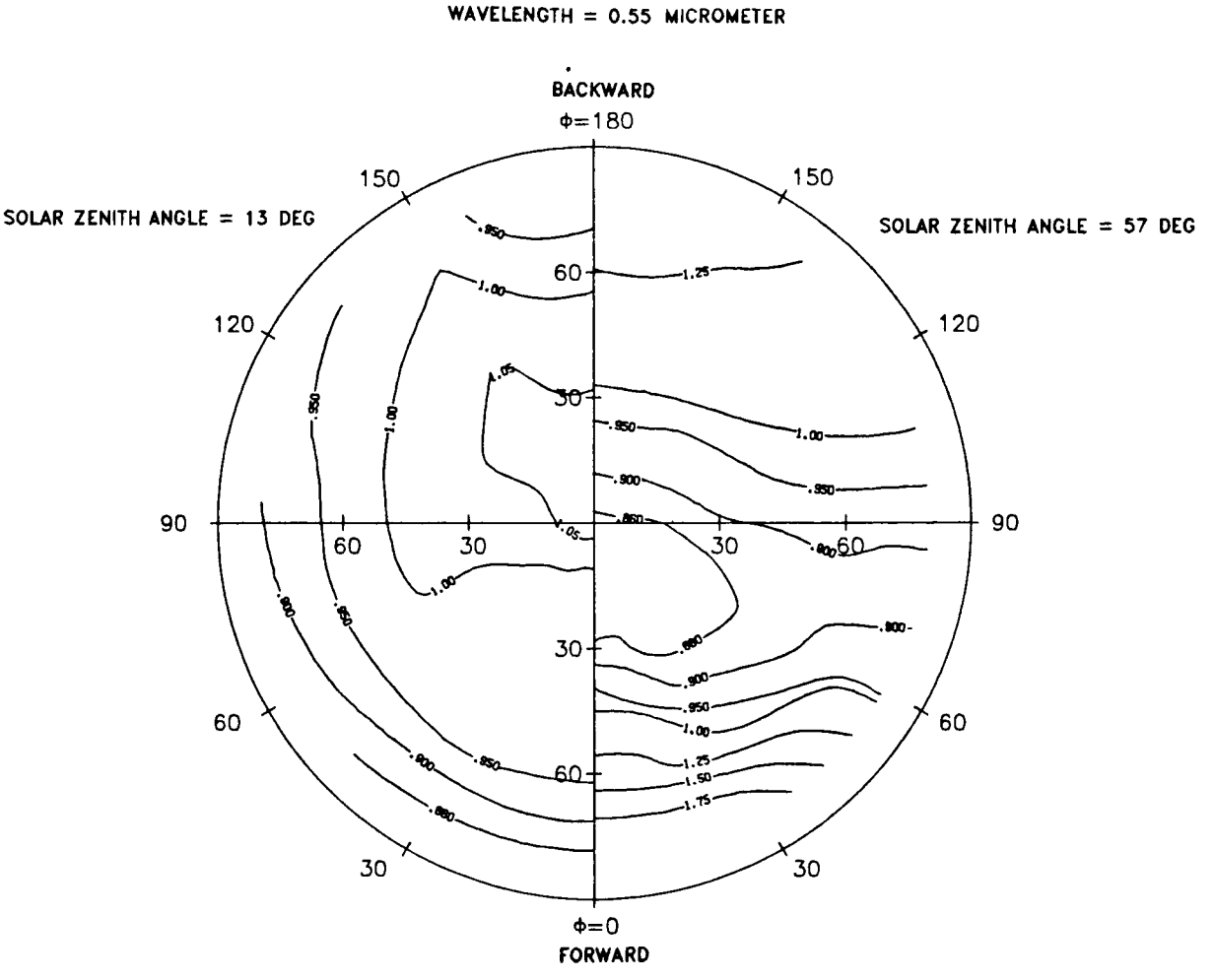

Figure 16. Ratio of anisotropic reflectance factor to albedo for Sonora Desert.

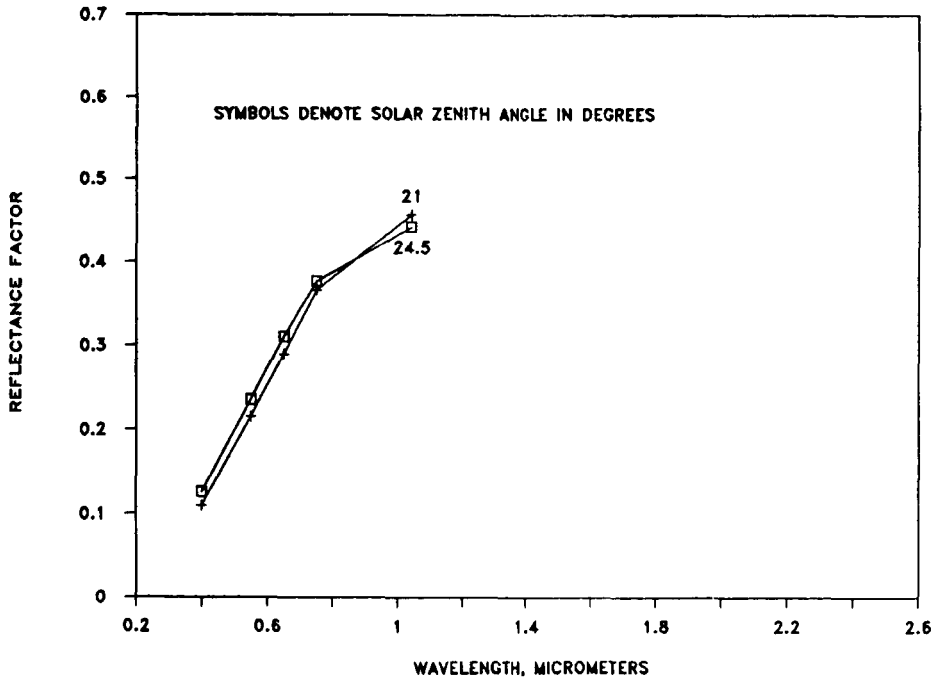

(a) Mohawk Valley reflectance.

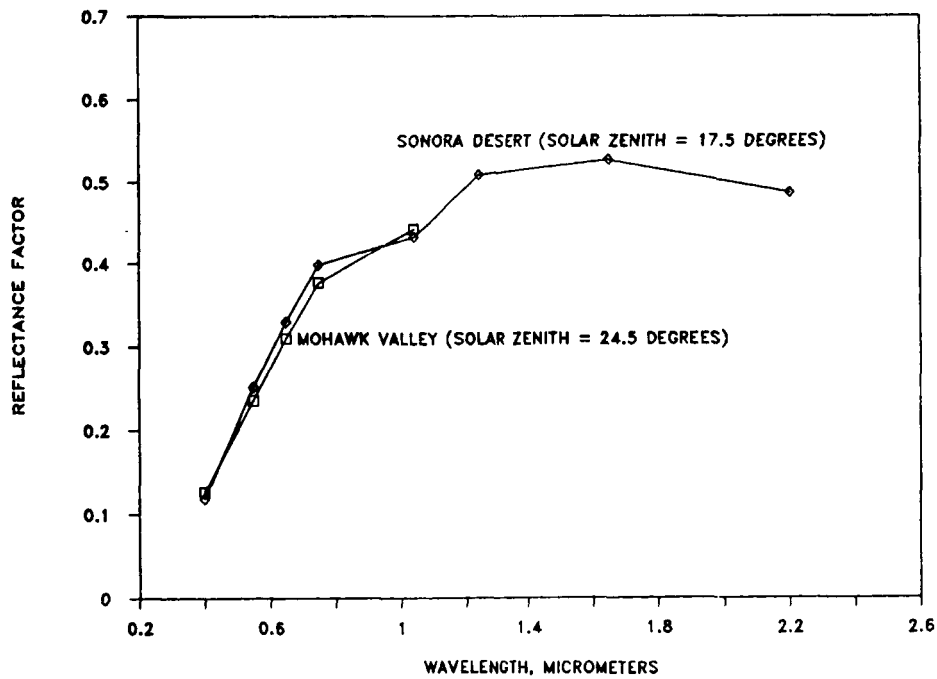

(b) Sonora-Mohawk comparison.

Figure 17. Nadir reflectance for Mohawk Valley.

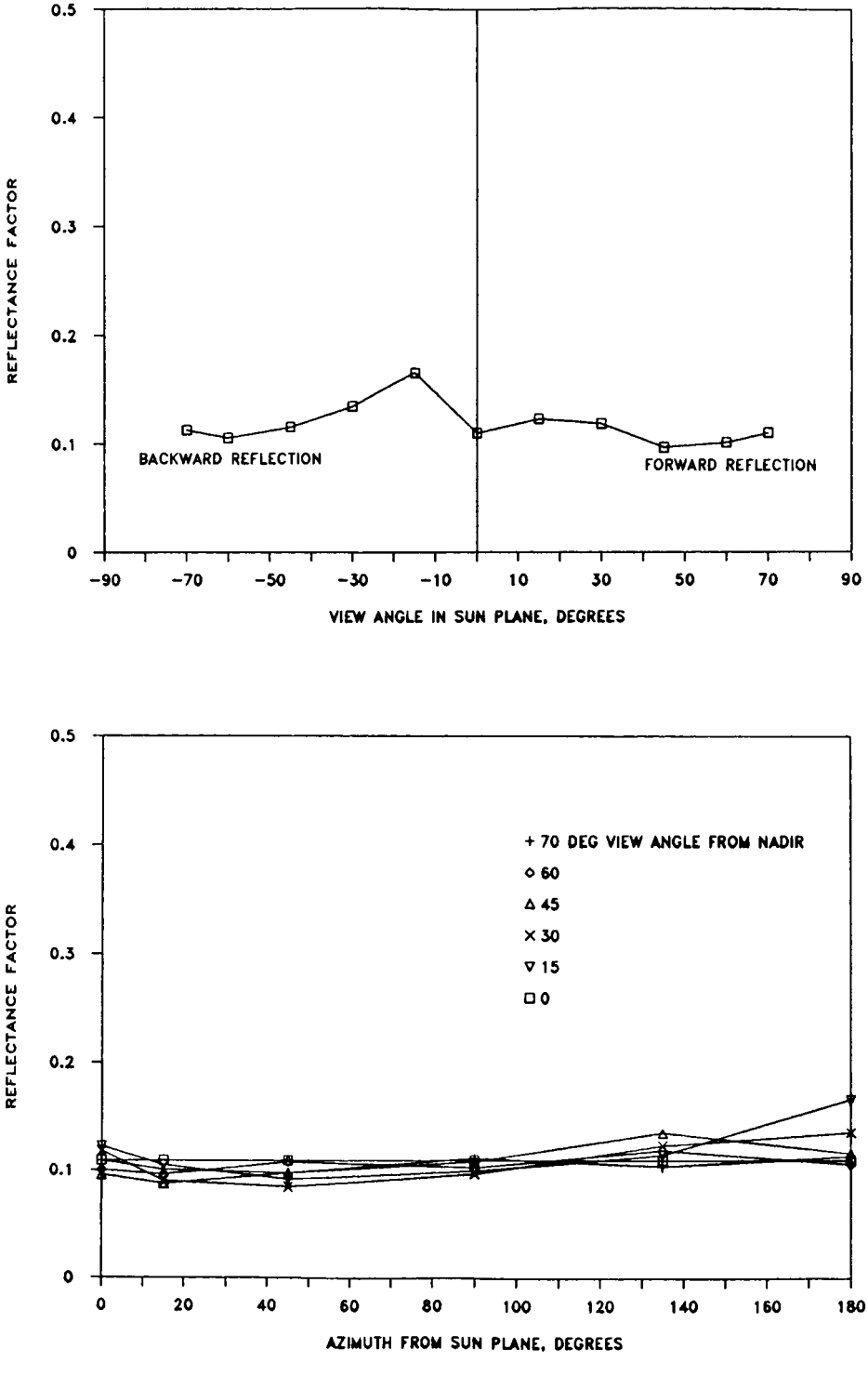

(a) Wavelength, 0.4 μm.

Figure 18. Bidirectional reflectance for Mohawk Valley.

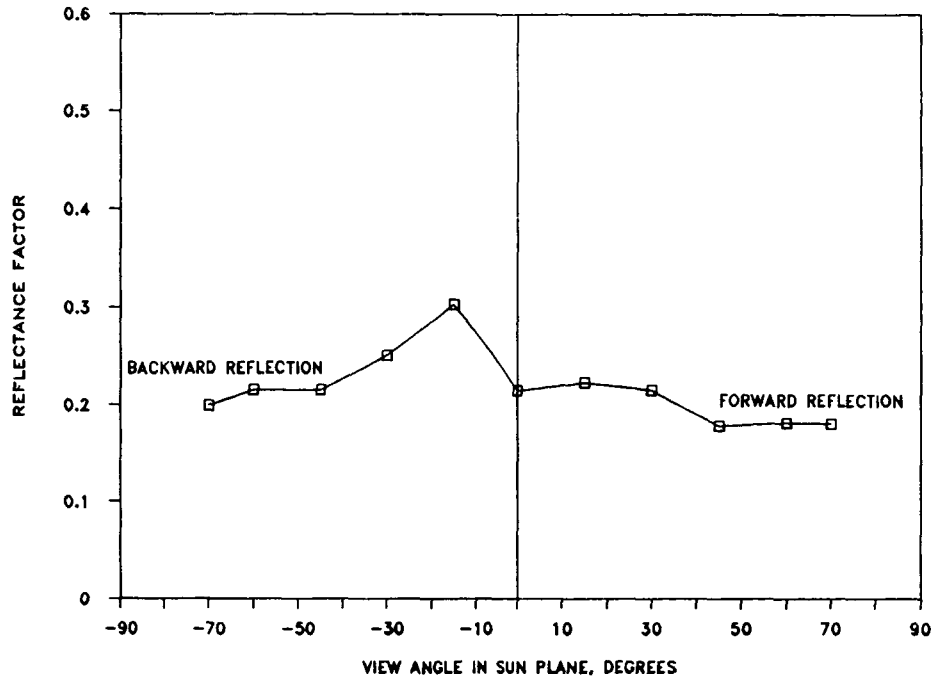

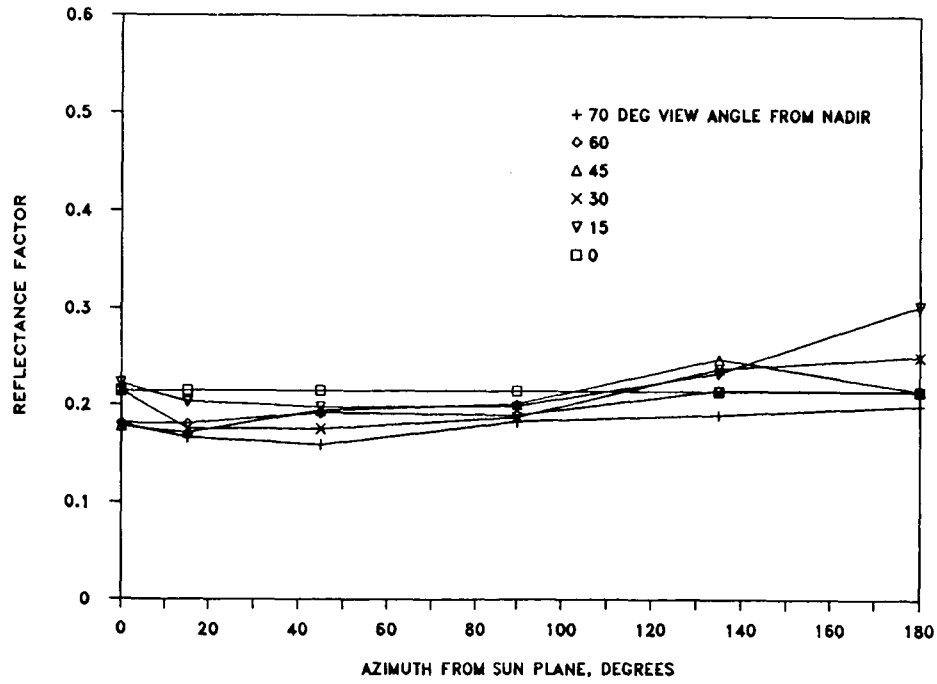

(b) Wavelength, 0.55 μm.

Figure 18. Continued.

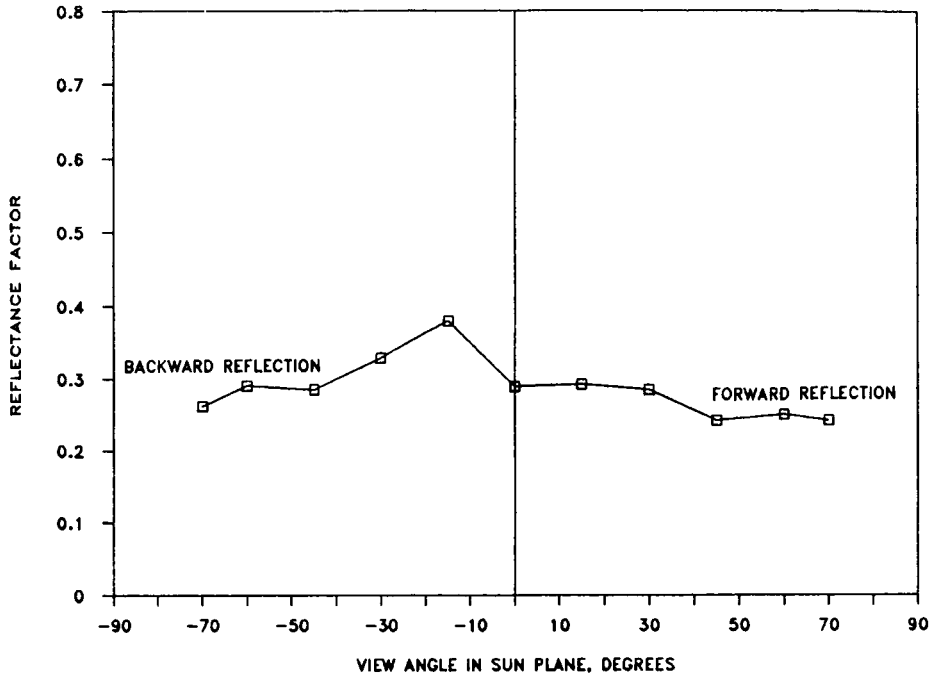

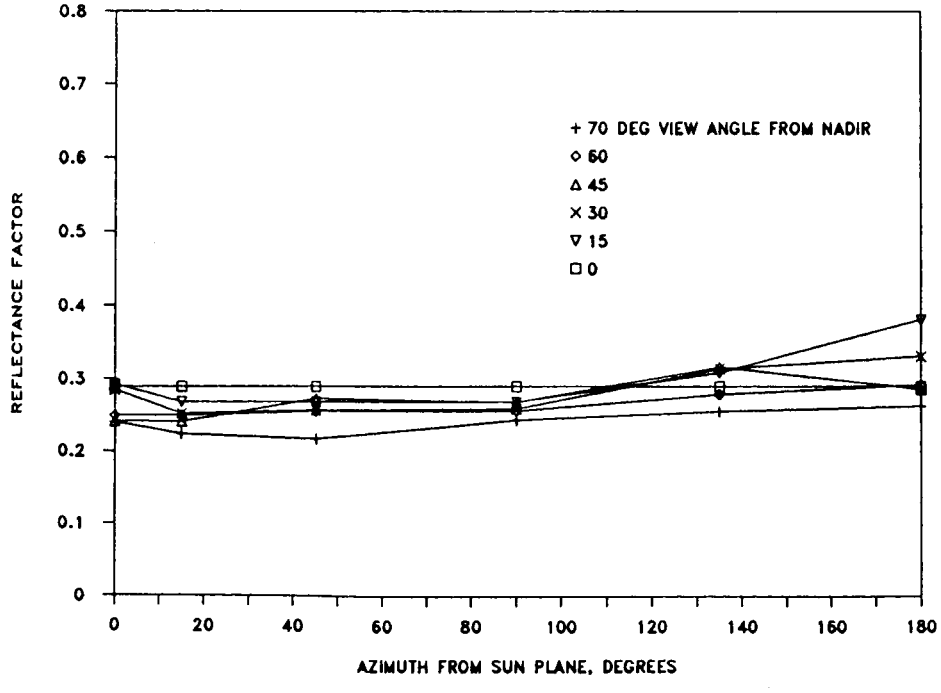

(c) Wavelength, 0.65 μm.

Figure 18. Continued.

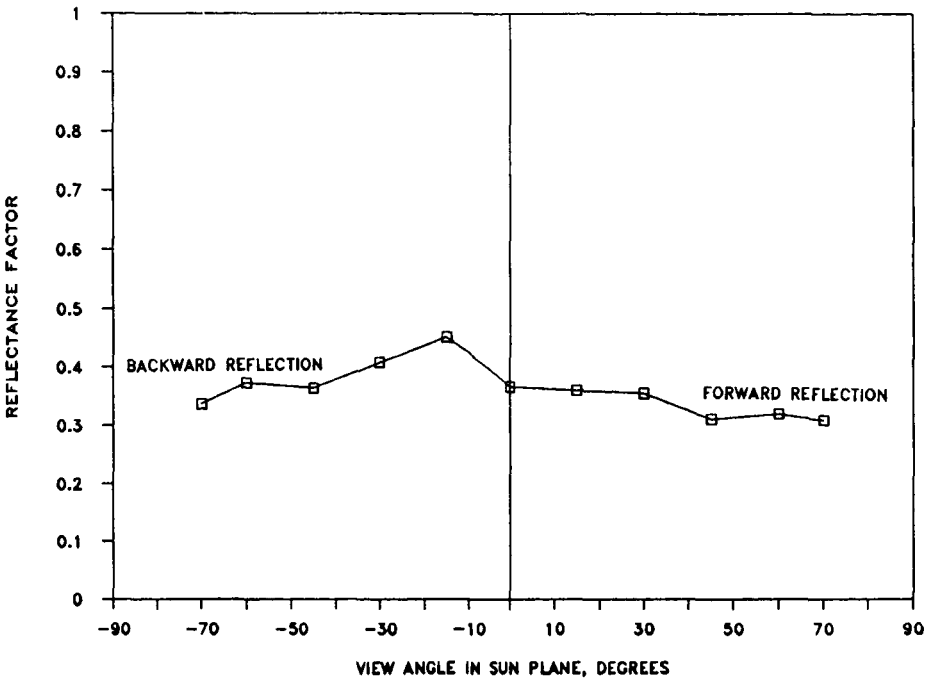

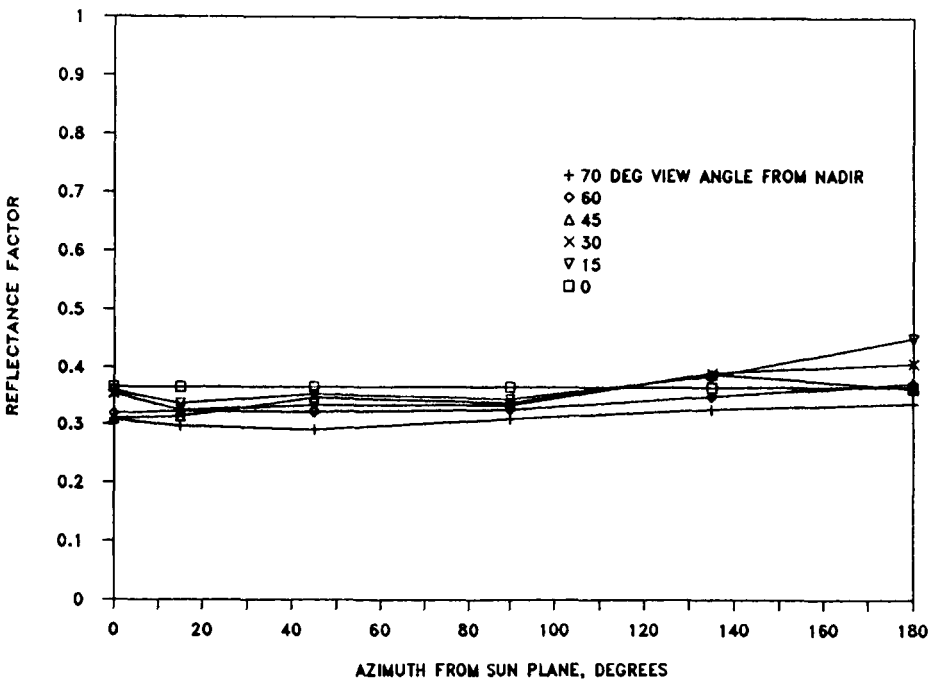

(d) Wavelength, 0.75 μm.

Figure 18. Continued.

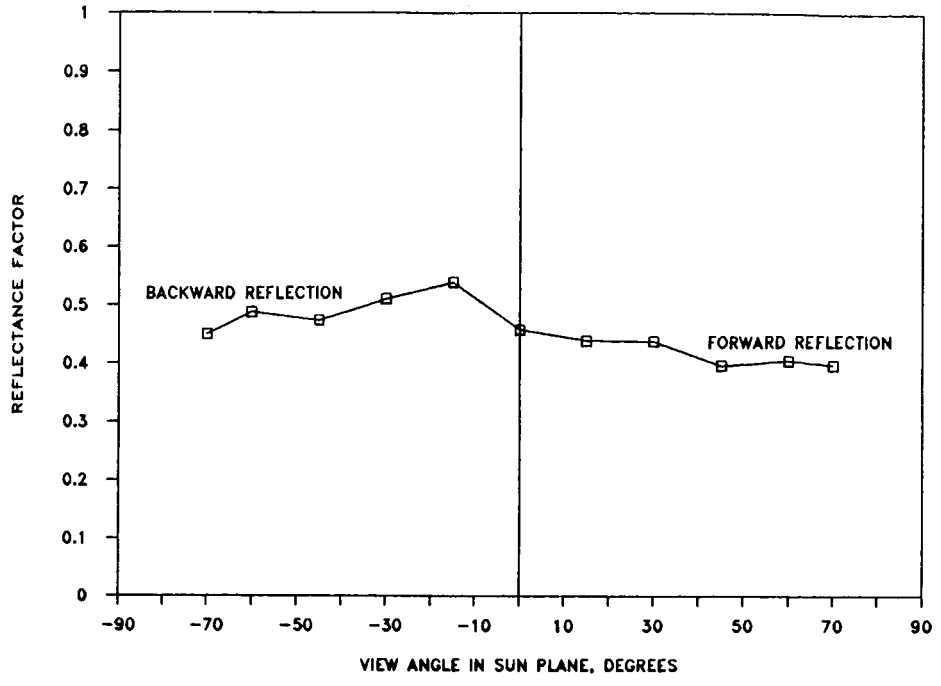

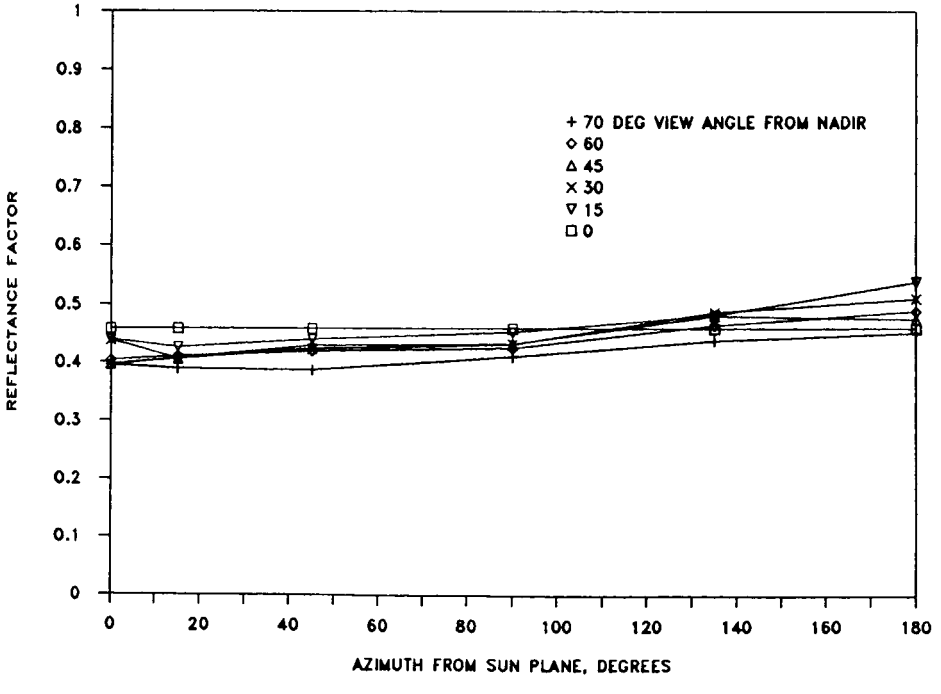

(e) Wavelength, 1.04 μm.

Figure 18. Concluded.

NASA
National Aeronautics and Space Administration

Report Documentation Page

1. Report No.	2. Government Accession No.	3. Recipient's Catalog No.
NASA TP-2643		

4. Title and Subtitle	5. Report Date
Surface Bidirectional Reflectance Properties of Two Southwestern Arizona Deserts for Wavelengths Between 0.4 and 2.2 Micrometers	May 1987
	6. Performing Organization Code
7. Author(s)	8. Performing Organization Report No.
Charles H. Whitlock, G. Carlton Purgold, and Stuart R. LeCroy	L-16159
9. Performing Organization Name and Address	10. Work Unit No.
NASA Langley Research Center Hampton, VA 23665-5225	672-40-04-70
	11. Contract or Grant No.
12. Sponsoring Agency Name and Address	13. Type of Report and Period Covered
National Aeronautics and Space Administration Washington, DC 20546-0001	Technical Paper
	14. Sponsoring Agency Code

15. Supplementary Notes

16. Abstract

Surface bidirectional reflectance characteristics are presented for the Sonora Desert and the Mohawk Valley at solar zenith angles of 13°, 31°, and 57° at wavelengths between 0.4 and 1.6 μm. Nadir reflectance values are presented for wavelengths between 0.4 and 2.2 μm for solar zenith angles of 13°, 17.5°, 27°, 31°, 45°, 57°, and 62°. Data were taken from a helicopter during May 1985 in support of an Earth Radiation Budget Experiment (ERBE), a Stratospheric Aerosol Gas Experiment (SAGE II), and an Advanced Very High Resolution Radiometer (AVHRR) satellite validation experiment.

17. Key Words (Suggested by Authors(s))

Albedo
Desert
Sonora Desert
Reflectance
Bidirectional reflectance

18. Distribution Statement

Unclassified—Unlimited

Subject Category 43

19. Security Classif.(of this report)	20. Security Classif.(of this page)	21. No. of Pages	22. Price
Unclassified	Unclassified	45	A03

For sale by the National Technical Information Service, Springfield, Virginia 22161-2171